Annual Technical Report

Research Related to the Development, Fabrication and Characterization of UV Detectors and Cold Cathode Devices

Supported under Grant #N00014-96-1-0765
Office of the Chief of Naval Research
Report for the period 5/1/96–12/31/96

R. F. Davis, M. D. Bremser, D. Hanser, O. H. Nam,
W. Perry and S. Smith
North Carolina State University
Materials Science and Engineering Department
Box 7907
Raleigh, NC 27695

December, 1996

DISCLAIMER NOTICE

THIS DOCUMENT IS BEST QUALITY AVAILABLE. THE COPY FURNISHED TO DTIC CONTAINED A SIGNIFICANT NUMBER OF PAGES WHICH DO NOT REPRODUCE LEGIBLY.

REPORT DOCUMENTATION PAGE

Form Approved
OMB No. 0704-0188

1. AGENCY USE ONLY *(Leave blank)*	2. REPORT DATE	3. REPORT TYPE AND DATES COVERED
	December, 1996	Annual Technical 5/1/96-12/31/96

4. TITLE AND SUBTITLE

Research Related to the Development, Fabrication and Characterization of UV Detectors and Cold Cathode Devices

5. FUNDING NUMBERS

s400003srr14
1114SS
N00179
N66005
4B855

6. AUTHOR(S)

R. F. Davis

7. PERFORMING ORGANIZATION NAME(S) AND ADDRESS(ES)

North Carolina State University
Hillsborough Street
Raleigh, NC 27695

8. PERFORMING ORGANIZATION REPORT NUMBER

N00014-96-1-0765

9. SPONSORING/MONITORING AGENCY NAMES(S) AND ADDRESS(ES)

Sponsoring: ONR, Code 312, 800 N. Quincy, Arlington, VA 22217-5660
Monitoring: Admin. Contracting Officer, ONR, Regional Office Atlanta
101 Marietta Tower, Suite 2805
101 Marietta Street
Atlanta, GA 30323-0008

10. SPONSORING/MONITORING AGENCY REPORT NUMBER

11. SUPPLEMENTARY NOTES

12a. DISTRIBUTION/AVAILABILITY STATEMENT

Approved for Public Release; Distribution Unlimited

12b. DISTRIBUTION CODE

13. ABSTRACT ***(Maximum 200 words)***

Selective growth of GaN and $Al_{0.2}Ga_{0.8}N$ has been conducted on stripe and circular patterned GaN/AlN/6H-SiC(0001) multilayer substrates. Prismatic morphology with (1-101) side facets was observed on 3 μm wide stripes for both materials. Hexagonal pyramid arrays of undoped GaN and Si-doped GaN were achieved on 5 μm circular patterns. Field emission measurements of the resulting Si-doped GaN pyramids exhibited a turn-on field of 25V/μm for an emission current of 10.8 nA at an anode-to-sample distance of 27 μm. Thin films of Si doped $Al_xGa_{1-x}N$ ($0.03 \leq x \leq 0.42$) were deposited on on-axis 6H-SiC(0001) substrates at 1100°C using a 0.1μm AlN buffer layer for electrical isolation. Hall effect and CL measurements were used to characterize the electrical and optical properties of these films, respectively. Alloys having the compositions of $Al_{0.08}Ga_{0.92}N$ and $Al_{0.42}Ga_{0.58}N$ exhibited mobilities of 110 and 14 $cm^2/V{\cdot}s$ at a carrier concentrations of 9.6e18 and 5.0e17 cm^{-3}, respectively. Acceptor doping of $Al_xGa_{1-x}N$ for $x \leq 0.08$ was also achieved for films deposited at 1050°C. The growth of GaN and $In_{0.22}Ga_{0.27}N$ thin films on 6H-SiC(0001) substrates each containing a high temperature AlN buffer layer has been achieved using a second and more novel OMVPE reactor designed specifically to improve the flow dynamics of the film deposition process. Donor (Si) doping of GaN was achieved with doping levels of 5E16 - 3E18 cm^{-3}. Growth of GaN in H_2 and N_2 was accomplished with the two main differences being stronger PL intensity and slower growth rate for the films grown in N_2. Narrow and bright photoluminescence was observed both at room temperature and 12 K. Biaxial strains resulting from mismatches in thermal expansion coefficients and lattice parameters in 22 GaN films grown on AlN buffer layers previously deposited on vicinal and on-axis 6H-SiC(0001) substrates were measured via changes in the c-axis lattice parameter. A Poisson's ratio of n=0.18 was calculated. The bound exciton energy (E_{BX}) was a linear function of these strains. The shift in E_{BX} with film stress was 23 meV/GPa. Threading dislocations densities of ~$10^{10}/cm^2$ and ~$10^8/cm^2$ were determined for GaN films grown on vicinal and on-axis SiC, respectively. A 0.9% residual compressive strain at the GaN/AlN interface was observed by HRTEM. A new inductively coupled plasma (ICP) system has been designed, fabricated and initially tested. Parametric studies involving process gas flow rates, ICP and RF bias power and pressure to optimize the system for fast etch rates with the least surface damage/ contamination are ongoing. Schottky contacts will be used to characterize the resulting electrical characteristics.

14. SUBJECT TERMS

GaN, AlN, $Al_xGa_{1-x}N$, InGaN, thin films, selective growth, pyramid arrays, field emission, doping, photoluminescence, Biaxial strain, thermal expansion coefficient, lattice parameter, Poisson's ratio, bound exciton, threading dislocations, inductively coupled plasma, Schottky contacts, HRTEM

15. NUMBER OF PAGES

46

16. PRICE CODE

17. SECURITY CLASSIFICATION OF REPORT	18. SECURITY CLASSIFICATION OF THIS PAGE	19. SECURITY CLASSIFICATION OF ABSTRACT	20. LIMITATION OF ABSTRACT
UNCLAS	UNCLAS	UNCLAS	SAR

I. Introduction

The numerous potential semiconductor applications of the wide band gap III–nitrides has prompted significant research regarding their growth and development. Gallium nitride (wurtzite structure), the most studied in this group, has a bandgap of ≈3.4 eV and forms continuous solid solutions with both AlN (6.2 eV) and InN (1.9 eV). As such, materials with engineered band gaps are feasible for optoelectronic devices tunable in wavelength from the visible to the deep UV. The relatively strong atomic bonding of these materials also points to their application for high-power and high-temperature microelectronic devices. Diodes emitting light from the yellow into the blue regions of the spectrum, blue emitting lasers, and several types of high-frequency and high-power devices have recently been fabricated from these materials.

Single crystal wafers of GaN are not commercially available. Sapphire(0001) is the most commonly used substrate, although its lattice parameter and coefficients of thermal expansion are significantly different from that of any III-nitride. The heteroepitaxial nucleation and growth of monocrystalline films of GaN on any substrate and AlN on sapphire are difficult at elevated (>900°C) temperatures. Therefore, at present, for successful organometallic vapor phase epitaxy (OMVPE) of GaN films on sapphire, the use of the initial deposition of an amorphous or polycrystalline buffer layer of AlN [1,2] or GaN [3,4] at low-temperatures (450°-600°C) is necessary to achieve both nucleation and relatively uniform coverage of the substrate surface. Subsequent deposition at higher temperatures and concomitant grain orientation competition has resulted in films of GaN(0001) and various nitrides alloys of improved quality and surface morphology relative to that achieved by growth directly on this substrate.

By contrast, we have observed that AlN and $Al_xGa_{1-x}N$ alloys containing even low ($x \geq 0.05$) concentrations of AlN deposited on 6H-SiC(0001) substrates at high (≥1000°C) temperatures undergo two-dimensional nucleation and growth with resulting uniform surface coverage. In this research, the use of a 1000 Å, monocrystalline, high-temperature (1100°C) AlN buffer has resulted in GaN films void of oriented domain structures and associated low-angle grain boundaries [5,6]. Monocrystalline films of $Al_xGa_{1-x}N$ ($0.05 \leq x \leq 0.70$) of the same quality have also been achieved at 1100°C.

The investigations to 1975 regarding III-Nitrides in terms of thin films growth, characterization, properties and device development have been reviewed by Kesamanly [7] and Pankove and Bloom [8]. The considerable progress accomplished in these areas in the intervening years has been reviewed in Refs. [9–16]. Research in the authors' group at NCSU employs both MOCVD and GSMBE to grow GaN and $Al_xGa_{1-x}N$ films on α(6H)-SiC(0001)$_{Si}$ substrates. Only the investigations involving the former technique are described herein.

Selective growth of particular microstructures have been used extensively for the fabrication of semiconductor devices such as quantum well, wire and dot structures, as well as

Table of Contents

I.	Introduction	1
II.	Selective Growth Via OMVPE of and Field Emission from GaN and $Al_{0.2}Ga_{0.8}N$ Pyramids on GaN/AlN/6H-SiC(0001) Multilayer Substrates *O. H. Nam and M. D. Bremser*	3
III.	Acceptor and Donor Doping of $Al_xGa_{1-x}N$ Thin Films Alloys on 6H-SiC(0001) Substrates via Metalorganic Vapor Phase Epitaxy *M. D. Bremser*	9
IV.	Growth of III-V Nitride Thin Films on α(6H)-SiC(0001) Via Organometallic Vapor Phase Epitaxy *D. Hanser*	16
V.	Correlation of Biaxial Strains, Bound Exciton Energies, and Defect Microstructures in GaN Films Grown on AlN/6H-SiC(0001) Substrates *W. G. Perry*	24
VI.	Dry Etching of Gallium Nitride *S. Smith*	40
VII.	Distribution List	46

field emitter structures. The selective growth of GaN and $Al_{0.1}Ga_{0.9}N$ linear windows and GaN hexagonal pyramid arrays on dot-patterned GaN/sapphire substrates have been reported [17,18]. The first field emission from an undoped GaN hexagonal pyramid array on a GaN/sapphire substrate has also been observed [18], and the enhancement of field emission performance was recently reported [20]. Thus far, all research regarding selective growth of GaN has used sapphire substrates. However, in the present research, 6H-SiC substrates have been employed with excellent results.

In this reporting period, research has been conducted in the following areas: (1) selective growth of and field emission from GaN and $Al_xGa_{1-x}N$ pyramids on 6H-SiC substrates, (2) growth, doping and characterization of GaN, $Al_xGa_{1-x}N$ and $In_xGa_{1-x}N$ films on 6H-SiC substrates, (3) determination and correlation of biaxial strains, bound exciton energies and defect microstructures in GaN films, and (4) the application of the inductively coupled etching technique to produce device microstructures in GaN and AlN. The following sections are self-contained in that they provide an introduction, results, discussion of results, conclusions and references for a given topic.

References

1. M. A. Khan, J. N. Kuznia, D. T. Olson, and R. Kaplan, J. Appl. Phys. **73**, 3108 (1993).
2. H. Amano, I. Akasaki, K. Hiramatsu, N. Koide, and N. Sawaki, Thin Solid Films **163**, 415 (1988).
3. J. N. Kuznia, M. A. Khan, D. T. Olson, R. Kaplan and J. Freitas, J. Appl. Phys. **73**, 4700 (1993).
4. S. Nakamura, Jpn. J. Appl. Phys. **30**, L1705 (1991).
5. T. W. Weeks, Jr., M. D. Bremser, K. S. Ailey, E. P. Carlson, W. G. Perry, R. F. Davis, Appl. Phys. Lett. **67**, 401 (1995).
6. T. W. Weeks, Jr., M. D. Bremser, K. S. Ailey,W. G. Perry, E. P. Carlson, E. L. Piner, N. A. El-Masry, and R. F. Davis, J. Mat. Res. J. **11**, 1081 (1996).
7. F. P. Kesamanly, Sov. Phys. Semicond. **8**, 147 (1974).
8. J. I. Pankove and S. Bloom, RCA Rev. **36**, 163 (1975).
9. R. F. Davis, *et al.*, J. Mater. Sci. Eng. B **1**, 77 (1988).
10. S. Strite and H. Morkoc, J. Vac. Sci. Technol. B **10**, 1237 (1992).
11. J. I. Pankove, in *Diamond, Silicon Carbide and Related Wide Bandgap Semiconductor Materials*, edited by J. T. Glass, R. F. Messier, and N. Fujimori, (Mater. Res. Soc. Sym Proc. Vol. 116, Pittsburgh, PA, (1990), 515-524.
12. R. F. Davis, Proc. IEEE **79**, 702 (1991).
13. H. Morkoç, *et al.*, J. Appl. Phys. **76**, 1363 (1994).
14. J. H. Edgar, J. Mater. Res. **7**, 235 (1992).
15. M. Henin, J. Microelectron. **23**, 500 (1992).
16. H. Morkoç S. Strite, G. B. Gao, M. E. Lin, B. Sverdlov, B. and M. Burns, J. Appl Phys. **76**, 1363 (1994).
17. S. Kitamura, K. Hiramatsu and N. Sawaki, Jpn. J. Appl. Phys. **34**, 2284 (1995).
18. R. D. Underwood, D. Kapolnek, B. P. Keller, S.Keller, S. P. DenBaars and U. K. Mishra, Topical Workshop on Nitrides, Nagoya, Japan, September (1995).
19. T. Tanaka, K. Uchida, A. Watanabe and S. Minagawa, Appl. Phys. Lett. **68**, 976 (1996).

II. Selective Growth Via OMVPE of and Field Emission from GaN and $Al_{0.2}Ga_{0.8}N$ Pyramids on GaN/AlN/6H-SiC(0001) Multilayer Substrates

A. Introduction

Wide band gap III-nitrides are being extensively studied for application in optoelectronic and microelectronic devices, including field emitter. Gallium nitride is a promising material in this group for field emitters because of its low electron affinity (2.7-3.3eV) [1, 2], high thermal, chemical and mechanical stability as well as the ability for controlled n-type doping. A recent report, in which AlN and Al-rich $Al_xGa_{1-x}N$ films have been shown to have a negative electron affinity, suggests these materials could be key elements of field emitters [2, 3].

Selective growth techniques are available not only for the fabrication of semiconductor devices such as quantum well wire and dot structures, but also for field emitters. The selective growth of GaN and $Al_{0.1}Ga_{0.9}N$ on linear windows and GaN hexagonal pyramid fabrication on dot-patterned GaN/sapphire substrates by this technique have been reported [4, 5]. The first field emission and the enhancement of this phenomenon from an undoped GaN hexagonal pyramid array on a GaN/sapphire substrate have been observed [6, 7]. In a related area, the selective growth of GaN layers on sapphire substrates has been reported for low-loss optical wave guide structures for active and passive photonic devices [8]. To date, all research on the selective growth of GaN have used sapphire substrates. In this paper, the selective growth of GaN and $Al_{0.2}Ga_{0.8}N$ on stripe patterned GaN/AlN/6H-SiC(0001) multilayer substrates via organometallic vapor phase epitaxy is reported. These substrates were produced using techniques described elsewhere [9, 10]. For the first time, fabrication of GaN and Si-doped GaN hexagonal pyramid arrays on circular patterns and the field emission results from these arrays is reported.

B. Experimental Procedures

The selective growth of GaN and $Al_{0.2}Ga_{0.8}N$ was performed on stripe (window width = 3-80μm) and circular (diameter = 5μm) patterned GaN/AlN/6H-SiC(0001) multilayer substrates. To produce these substrates, undoped or Si-doped GaN films (n = 2E18cm^{-3}) having a thickness of 1.5μm were first grown on a high temperature AlN buffer layer on a 6H-SiC(0001) substrate in a cold-wall, vertical, pancake-style, RF inductively heated OMVPE system. The experimental growth parameters are described elsewhere [9, 10]. A SiO_2 mask layer (thickness=1000Å) was subsequently deposited on each multilayer substrate by RF sputtering or LPCVD. Patterning of the mask layer was achieved using standard photolithography techniques and etching with a buffered HF solution. In the stripe patterned samples, the edges of the stripes were parallel to the <11-20> direction. Prior to selective

growth, the patterned samples were dipped in a buffered HCl solution to remove the surface oxide of the underlying GaN layer.

Selective growth was conducted at 1000–1050°C and 45 Torr. Triethylgallium (TEG), triethylaluminium (TEA) and 1500 sccm NH_3 were used in combination with a 3000 sccm H_2 diluent. The ratio of NH_3 and TEG was varied from 960 to 2600. Silicon was incorporated into the GaN hexagonal pyramids during the selective growth using SiH_4 at a flow rate of 5.5nmol/min. The morphologies of the selectively grown samples were observed using scanning electron microscopy (SEM-JEOL 6400 FE). The final step was the deposition of Ti(200Å)/Au(1500Å) contacts via electron beam evaporation on Si-doped GaN layer.

The field emission measurements (FEM) were performed on the hexagonal pyramid arrays of Si-doped GaN in a UHV-FEM system having a working pressure of 2×10^{-8} Torr. During the measurement, samples were placed beneath a 5mm diameter movable Mo anode with a flat tip. The anode was controlled by a stepping motor such that one step yielded a translation of 0.44 μm. The current-voltage (I-V) measurements were taken at several distances ranging from 2 to 40 μm for anode voltages in the range of 0 to 1100 V.

C. Results and Discussion

The characteristics of the stripe patterns of deposited GaN and $Al_{0.2}Ga_{0.8}N$ having various window widths were determined using SEM as shown in the micrographs in Fig. 1. Both materials showed prismatic morphology with (1-101) side facets on the 3μm-wide stripes. Truncated prismatic growth with (0001) top facets and (1-101) side facets was observed on stripe patterns with widths greater than 5μm. Polycrystals of $Al_xGa_{1-x}N$ nucleate on the SiO_2 mask because of the chemical interaction between Al and SiO_2 [4], there is no, however, significant difference in the final growth morphology for the GaN and $Al_{0.2}Ga_{0.8}N$ patterns. Only a slight roughening of the (1-101) facets was observed for $Al_{0.2}Ga_{0.8}N$ selective growth. This is probably due to the poor selectivity of $Al_{0.2}Ga_{0.8}N$, that is, the deposition of polycrystalline material on the SiO_2 mask. No ridge growth was observed along the edge of the stripes, and the (0001) top facets were very smooth and flat regardless of the width of the stripes. This suggests that insignificant lateral vapor phase diffusion of the reactive species from the mask to the window area occurred during the selective growth. It is probably due to the large ratio (=0.5) of the window to the mask area, because lower values of this ratio induce more lateral vapor diffusion [11].

Figure 2 shows SEM images of GaN grown on 5μm-wide stripe patterns using different flow rates of TEG. The higher flow rate of TEG resulted in a smaller area of (0001) top facets and the development of (1-101) side facets. This behavior supports the model that GaN selective growth depends on the balance between the incoming flux on the (0001) top facets

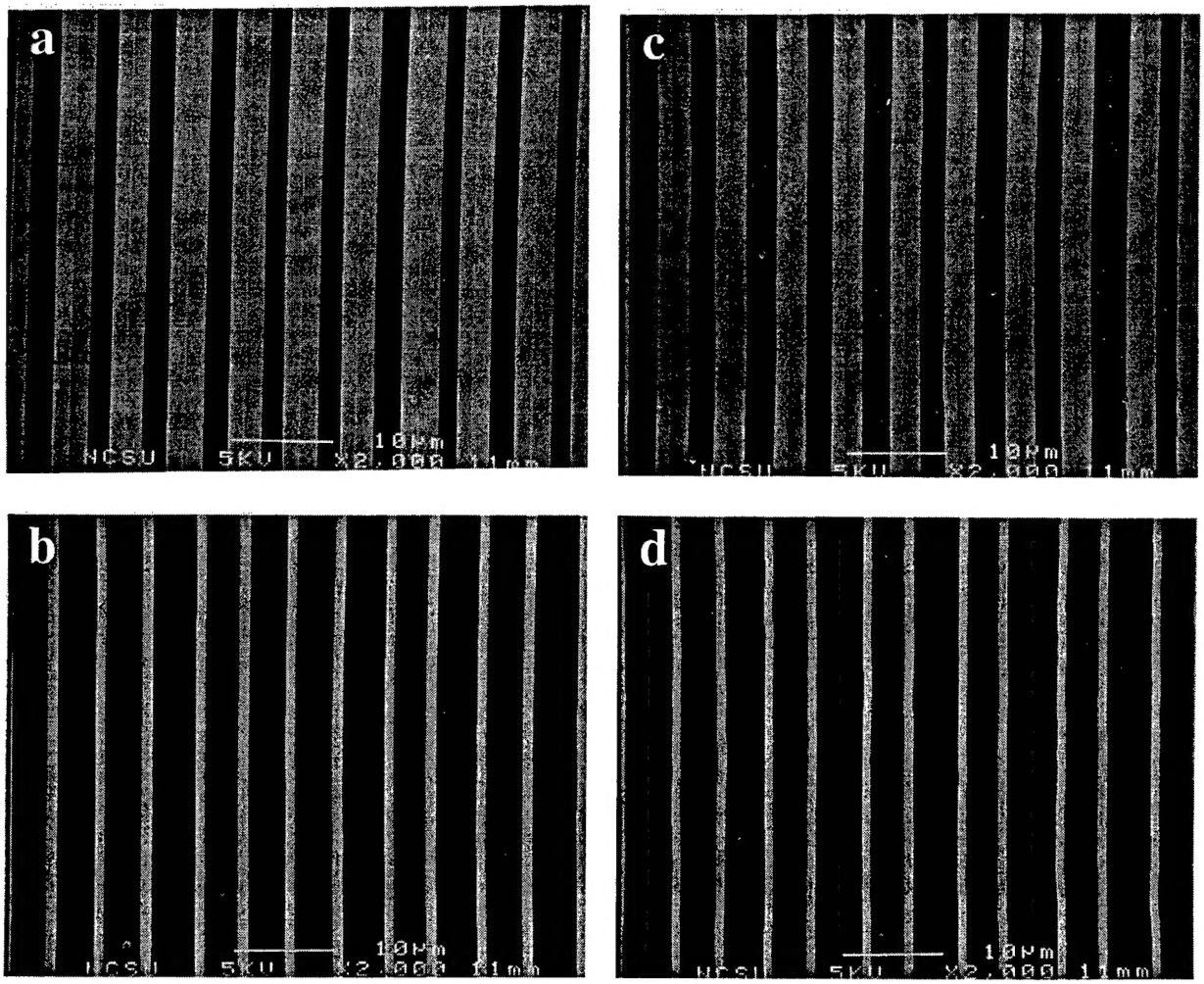

Figure 1. SEM micrographs of the selectively grown GaN (left) and $Al_{0.2}Ga_{0.8}N$ (right) layers on different wide-stripe patterns. (a-b) 3μm, (c-d) 5 μm.

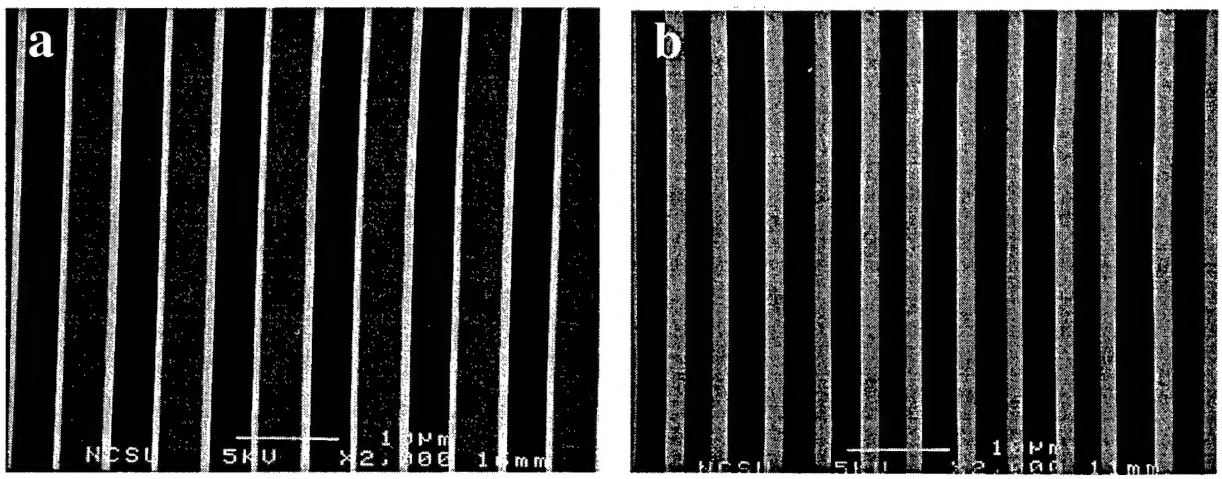

Figure 2. SEM micrographs of the selectively grown GaN layers on 5μm wide-stripe patterns at different flow rates of TEG. (a) 26μmol/min. (b) 70μmol/min.

and the outgoing flux from the (0001) to the (1-101) side facets [5]. Increased TEG flow rate promotes two-dimensional nucleation on the (0001) top facets, thereby reducing the surface diffusion length of the Ga adatoms. As a result, the growth rate of the (0001) facets becomes faster than that of the (1-101) facets.

The optimum conditions for selective growth of GaN hexagonal pyramids on circular patterns was based on the selective growth conditions on stripe patterns. The height of a hexagonal pyramid can be easily calculated by the relation of $H=D\cdot\tan 62^\circ/2$, where H and D are the height and the diagonal width of the base of the pyramid. Each pyramid has six (1-101) side facets. The growth rate of these pyramids is strongly dependent upon the ratio of window-to-mask area in the patterned region as well as the selective growth conditions. The average diagonal width of the pyramids was 7.7μm using a ratio of 0.1. However, increasing the ratio to 0.23 resulted in an average diagonal width of 5.7μm for the same growth condition. These results indicate that the lateral diffusion of the reactive species from the mask to the window area is also an important factor for the fabrication of GaN hexagonal pyramids. As shown in Fig. 3(a), the growth of an uniform array of Si-doped GaN hexagonal pyramid in an area of $0.5\times0.5mm^2$ was achieved for the first time. The high magnification SEM image shown in Fig. 3(b) reveals that the tip radius of the pyramids is less than 100nm.

Field emission measurements (FEM) of the Si-doped GaN pyramid arrays were conducted using a UHV-FEM system. The emission current was measured as a function of the anode voltage applied to a Mo rod. The I-V curve in Fig. 4(a) shows the turn-on voltage of 680V for a current of 10.8nA at a distance of 27μm between the pyramid array and the anode. This turn-on voltage corresponds to a turn-on field of 25V/μm. Using the same system, a polycrystalline p-type diamond film ($p = 2.5E17cm^{-3}$) grown on Si(100) exhibited a turn-on field intensity of

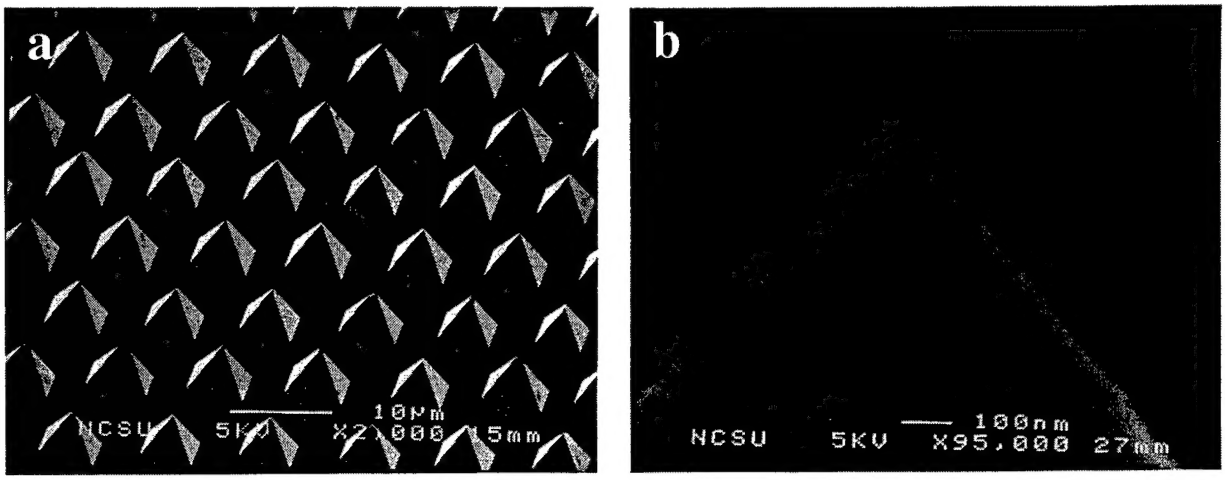

Figure 3. (a) SEM micrograph of Si doped GaN hexagonal pyramid array. (b) High magnification SEM image of the apex of a hexagonal pyramid. Tip radius is less than 100nm.

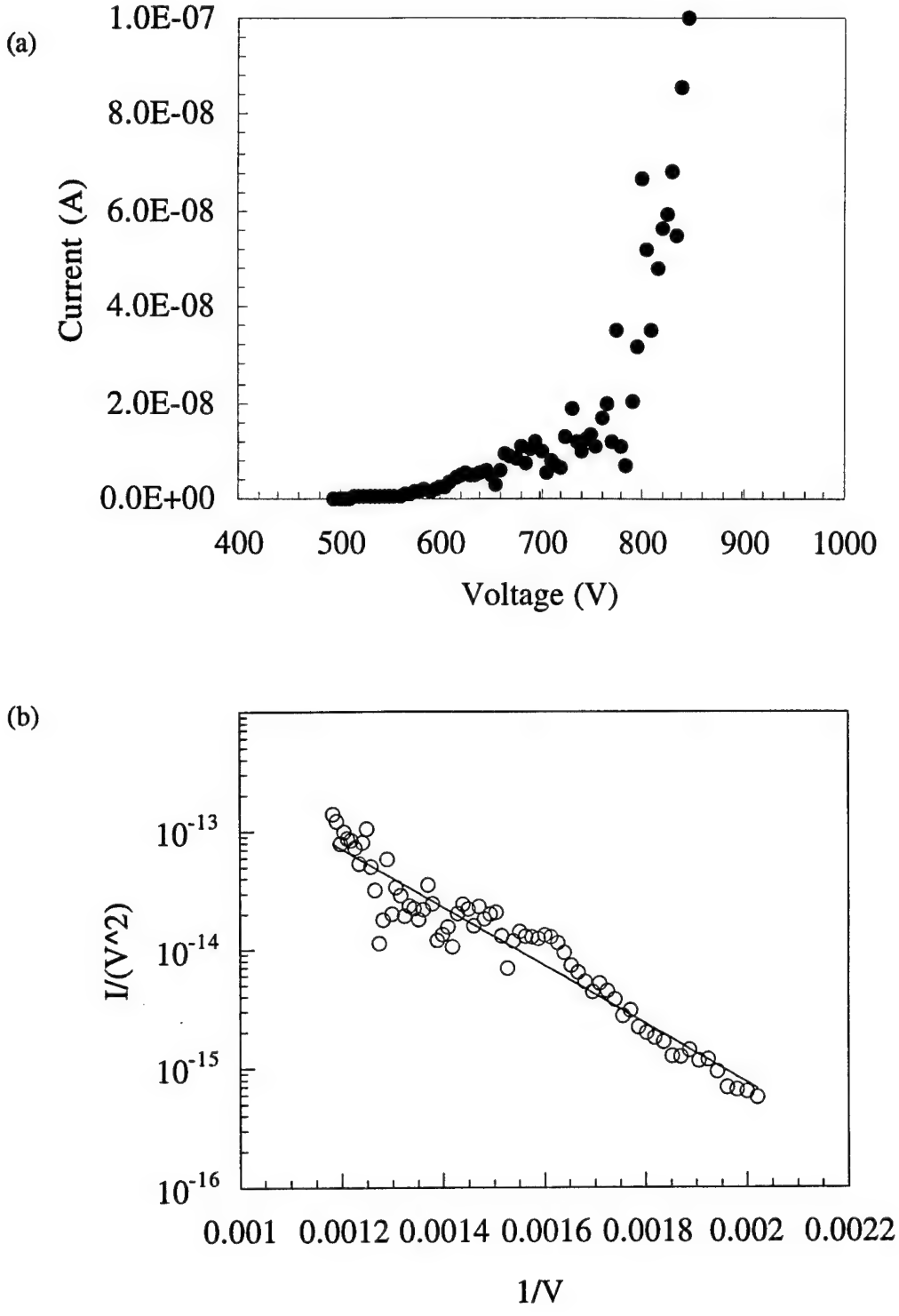

Figure 4. (a) Emission current and anode voltage characteristic of Si doped GaN hexagonal pyramid array. (b) Fowler-Nordheim plot of the I-V data. The straight line indicateds F-N tunneling.

27V/μm. The Fowler-Nordheim (F-N) plot obtained from the I-V data as shown in Fig. 4(b) reveals a linear relationship. This indicates that the emission from the Si-doped GaN array

obeys F-N field emission theory. Research is in progress to reduce the turn-on field of the Si-doped GaN arrays to several volts per μm in order to be considered for practical applications.

D. Conclusions

The selective growth of GaN and $Al_{0.2}Ga_{0.8}N$ has been conducted on stripe and circular patterned GaN/AlN/6H-SiC(0001) multilayer substrates. Prismatic morphology with (1-101) side facets was observed on 3μm wide stripes for both materials. Truncated prismatic growth with (0001) top facets and (1-101) side facets were obtained on stripe patterns with widths greater than 5μm. No ridge growth was observed along the edges of the stripe patterns and the (0001) top facets were very smooth and flat. Polycrystalline $Al_xGa_{1-x}N$ were deposited on the SiO_2 mask. For GaN selective growth on the stripe patterns, the increase of TEG flow rate resulted in the development of (1-101) side facets. Uniform hexagonal pyramid arrays of Si-doped GaN were successfully grown on circular patterns having diameters of 5μm. Field emission measurements of these arrays showed a turn-on field was 25V/μm for an emission current of 10.8nA at an anode-to-pyramid array distance of 27μm.

E. References

1. J. L. Shaw, H. F. Gray, K. L. Jensen, J. M. Jung, J. Vac. Sci. Technol. **B14**, 2072 (1996).
2. R. J. Nemanich, M. C. Benjamin, S. P. Bozeman, M. B. Bremser, S. W. King, B. L. Ward, R. F. Davis, B. Chen, Z. Zhang and J. Bernholc, MRS Fall Meeting, Boston, November (1995).
3. M. C. Benjamin, C. Wang, R. F. Davis and R. J. Nemanich, Appl. Phys. Lett. **64**, 3288 (1994).
4. Y. Kato, S. Kitamura, K. Hiramatsu and N. Sawaki, J. Crystal. Growth **144**, 133 (1994).
5. S. Kitamura, K. Hiramatsu and N. Sawaki, Jpn. J. Appl. Phys. **34**, 1184 (1995).
6. R. D. Underwood, D. Kapolnek, B. P. Keller, S. Keller, S. P. DenBaars and U. K. Mishra, Topical Workshop on Nitrides, Nagoya, Japan, September (1995).
7. R. D. Underwood, D. Kapolnek, B. P. Keller, S. Keller, S. P. DenBaars and U. K. Mishra, Solid State Electron., Submitted.
8. T. Tanaka, K. Uchida, A. Watanabe and S. Minagawa, Appl. Phys. Lett. **68**, 976 (1996).
9. T. W. Weeks Jr., M. D. Bremser, K. S. Ailey, E. P. Calson, W. G. Perry and R. F. Davis, Appl. Phys. Lett. **67**, 401 (1995).
10. M. D. Bremser, W. G. Perry, T. Zheleva, N. V. Edward, O. H. Nam, N. Parich, D. E. Aspnes and R. F. Davis, MRS Internet J. Nitride Semicond. Res. **1**, 8 (1996).
11. K. Yamaguchi and K. Okamoto, Jpn. J. Appl. Phys. **32** 1523 (1993).

III. Acceptor and Donor Doping of $Al_xGa_{1-x}N$ Thin Films Alloys on 6H-SiC(0001) Substrates via Metalorganic Vapor Phase Epitaxy

A. Introduction

The potential and realized employment of III-nitride materials for both optoelectronic and microelectronic applications has stimulated considerable research [1]. The wurtzitic phase of GaN forms a continuous solid solution with AlN; thus, materials having bandgaps from 3.4 eV to 6.2 eV can and have been produced. The $Al_xGa_{1-x}N$ solid solutions are of interest for use in ultraviolet emitters [2] and detectors [3], as well as high electron mobility transistors [4,5].

A principal focus in the area of epitaxial growth of III-N thin films is the marked reduction in the density of line and planar defects and point defects [6-12]. The densities of these extended defects are usually determined by substrate choice and the crystallography and microstructure of its surface, buffer layer choice, and the presence of impurities on the growing surface. The inclusion and the concentrations of point defects, e.g., impurities and native defects, are determined primarily by deposition conditions. Understanding and control of these point defects is critical in order to achieve the desired operational characteristics of nitride-based devices.

At present, Si and Mg are the most commonly employed donor- and acceptor-type dopants, respectively, for GaN. Therefore, it is logical that Si and Mg would likely be the most suited for doping $Al_xGa_{1-x}N$ alloys. For metalorganic vapor phase epitaxy (MOVPE) growth, the use of SiH_4 presents few complications; however, the conventional source of magnesium, Cp_2Mg, has been found troublesome. It is a solid source at room temperature which can lead to non-uniform transport to the growth chamber throughout the lifetime of the source. Moreover, the vapor is an unsaturated molecule which adsorbs to stainless steel causing memory affects. Additionally, it can bond with and transport oxygen into the growth chamber [13]. In MOVPE, decomposition of the metalorganics (MO) is the dominant source of carbon impurities while ammonia (NH_3) decomposition is a source of hydrogen. Moreover, in aluminum alkyls, the dominant impurity, dimethyaluminum-methoxide(DMAM) ($CH_3OAl(CH_3)_2$), is a source of oxygen contamination [14]. Upon transport to the growth chamber, decomposition allows for the incorporation of oxygen into the film. As the bubbler is depleted, the amount of oxygen transported to the chamber increases. Conversely, residual impurities in these alkyls, e.g., silicon decreases, since they tend to be incorporated in more volatile compounds which are transported earlier in the bubbler lifetime [15].

The concentrations of native defects such as antisites and vacancies are a strong function of growth conditions, particularly the substrate temperature and the V/III ratio. Additionally, the position of the Fermi level can strongly influence the existence of these defects which makes

them difficult to study. Although the estimation of their concentrations via state-of-the-art calculations are possible, quantitative determination is difficult. Usually implantation and annealing experiments are required for quantification. More frequently, variance of growth conditions, in conjunction with electrical and optical characterization, allows for the qualitative investigation of these defects. Similarly, quantification of impurity levels is extremely difficult in alloys since secondary ion mass spectroscopy (SIMS) is matrix dependence; thereby necessitating the fabrication of separate sets of standards for each alloy composition. It is also necessary to correlate these levels with electronic and optical properties in GaN and then apply these techniques to the investigation of alloy materials. In this research, doped and undoped $Al_xGa_{1-x}N$ ($x \leq 0.42$) deposited under various conditions has been characterized electrically and optically. These results will be discussed in light of recent theoretical studies.

B. Experimental Procedures

Thin films of $Al_xGa_{1-x}N$ were deposited on on-axis 6H-SiC(0001) substrates at 1050°C and 1100°C at 45 Torr using a vertical, cold-wall, RF inductively heated MOVPE deposition system. Deposition was performed using various ratios of triethylaluminum (TEA) and triethylgallium (TEG) in combination with 1.5 SLM of ammonia (NH_3) and 3 SLM of H_2 diluent. The total metalorganic precursor flow rate was 32.8 μmoles/min. A 0.1μm AlN buffer layer was used for Si-doped films to provide electrical isolation from the substrate. A 0.1 μm AlN/0.5 μm GaN buffer structure was used for Mg-doped samples, since p-type layers are usually the top layers in device structures. Donor- and acceptor-type doping of the alloys was accomplished by the addition of SiH_4 and Cp_2Mg, respectively. The Mg-doped samples were subsequently annealed by rapid thermal annealing (RTA) for 30s at 800°C. During annealing they were in contact with a Si wafer, and the temperature was measured by a calibrated thermocouple attached to the Si wafer. Films were characterized using scanning (SEM) and transmission (TEM) electron microscopies, photoluminescence (PL), cathodoluminescence (CL), capacitance-voltage (CV) measurements, Hall effect using the van der Pauw geometry at 293K and secondary ion mass spectroscopy (SIMS). Additional details regarding the experimental procedures are described elsewhere [16,17,18].

C. Results and Discussion

Scanning electron microscopy of the Si-doped $Al_xGa_{1-x}N$ films ($0.03 \leq x \leq 0.42$) revealed smooth, featureless surfaces under high magnification (40kX). Cathodoluminescence spectra of these films revealed strong, near-band edge (NBE) emission and a weak donor-to-acceptor (DA) transition located approximately 200 meV below the bandgap. Weak "yellow" emission was also present. The compositions of these films were estimated using EDX and the positions of the NBE CL emission. Although the previously published relationship of NBE CL emission

and composition (Eq.(1)) was for $Al_xGa_{1-x}N$ films deposited directly on SiC substrates [19], the differences in the calculated values of the Al mole fraction in those films and the films in the present study were within the limits of error (±2%) of the EDX analysis. Therefore, the slight blue shift in the NBE energy observed for $Al_xGa_{1-x}N$ films using an AlN buffer was neglected.

$$E_{I2}(x)=3.50 + 0.64x + 1.78x^2 \quad (1)$$

Results from Hall effect measurements for Si-doped $Al_xGa_{1-x}N$ grown with a constant Si flow rate are shown in Table I. The growth rate was determined to be about 0.5 μm/hr. for lower concentrations of Al (x=0.08) while films with higher Al concentrations (x=0.42) had a growth rate of about 0.35 μm/hr. Results from Si-doped GaN films (Group II) are included for comparison of the Hall mobilities.

For samples in Group I, small increases in the Al concentration greatly reduced the mobility of the donors. At 14% Al concentration, the mobility was reduced by more than 75% that of GaN having a similar donor concentration (Samples AlGaN:2 and GaN:4). At 42% Al composition, the Hall mobility was reduced by more than a factor of 20 over similarly doped GaN films (GaN:1 and GaN:2). Several reasons may be cited for these marked changes in electrical behavior: (1) alloy scattering, (2) donor level movement deeper into the gap and (3) formation of donor complex (DX) centers.

Alloy scattering (Mechanism 1) is certainly a potential reason for the lowered mobilities given the non-periodic potential created by the randomly placed Al and Ga atoms on the cation site in the lattice. Temperature dependent Hall measurements will be performed to verify the

Table I. Results of Hall Measurements on Si Doped and Undoped $Al_xGa_{1-x}N$ and GaN Thin Films

Sample ID	Composition (Al mole fraction)	Donors (cm^{-3})	Hall Mobility ($cm^2/V\ s$)	Resistivity (Ω-cm)
GROUP I (Si-doped)				
AlGaN:1	0.08	9.6e18	110	0.0062
AlGaN:2	0.14	9.9e18	41	0.015
AlGaN:3	0.24	2.6e18	76	0.031
AlGaN:4	0.32	1.1e18	51	0.11
AlGaN:5	0.42	5.0e17	14	0.90
GROUP II (Si-doped)				
GaN:1	-----	3.8e17	411	0.039
GaN:2	-----	6.4e17	309	0.031
GaN:3	-----	2.0e18	257	0.012
GaN:4	-----	1.1e19	170	0.0032

role of Mechanism 2. Silicon is shallow hydrogenic donor in GaN, but it is predicted to be a deep donor in AlN [20]. Mechanism 3 is a phenomena has been widely studied in $Al_xGa_{1-x}As$ [21]. Oxygen has been predicted to form a DX center in $Al_xGa_{1-x}N$ for alloys with a bandgap greater than 4.0 eV (x=0.35) [8]. This may contribute to the lower carrier concentrations and mobilities for alloys containing greater than 35% aluminum. Experimental results are needed to confirm this effect.

Acceptor doping of $Al_xGa_{1-x}N$ for $x \leq 0.08$ was also achieved for films deposited at 1050°C. Results of the CV measurements are shown in Table II. In general, it was found that it was necessary to *lower* the Cp_2Mg flow rate as the Al concentration increased. Samples with lower concentrations of Mg, exhibited better response to high frequency modulation (10^4, 10^5 Hz). This indicates that the more highly doped samples had a lower hole mobility [22]. Additionally, PL measurements of AlGaN:12 indicated no change in position in the commonly observed DA peak (2.88 eV at 4.2K) seen in highly Mg doped samples. Like GaN, lower Mg concentrations in $Al_xGa_{1-x}N$ films resulted in a shift to a higher energy PL transition [23, 24] Unlike GaN, whose higher energy PL transition is located at 3.27 eV at 4.2K, for $Al_{0.08}Ga_{0.12}N$ the higher energy PL transition was located 3.19 eV. The reason for this difference is unclear at this time.

In order to understand the Mg doped $Al_xGa_{1-x}N$, it is constructive to investigate and compare with Mg doped GaN (Table II). GaN:7 is an undoped film used for comparison. Capacitance-Voltage measurements revealed GaN:5 had a poorer response than GaN:6 to the applied small ac signal at 10^4 Hz. Only by reducing the small signal ac frequency to 10^3 Hz was a similar net ionized acceptor concentration measured as compared with GaN:6.

Photoluminescence revealed a strong DA luminescence peak centered at approximately 2.88 eV at 4.2K for both samples. More importantly, however, GaN:5 revealed an DA luminescence intensity 5 times strong than GaN:6. SIMS profiling for Mg, C, H, and O was performed on both samples as well an undoped sample. The results are shown in Table III.

Table II. Results of Capacitance-voltage Measurements on Mg Doped $Al_xGa_{1-x}N$ and GaN

Sample ID	Composition (Al mole fraction)	Cp_2Mg flow (nmol/min)	Net Ionized Acceptors N_A-N_D cm^{-3}
AlGaN:12	0.0350		1.5e19
AlGaN:13	0.06	25	2.0e19
AlGaN:14	0.06	25	1.0e19
AlGaN:15	0.08	15	1.5e18
AlGaN:16	0.08	7.5	3.0e18
GaN:5	-----	100	5.0e18
GaN:6	-----	50	1.5e19
GaN:7	-----	----	<1e16

Table III. Results of SIMS Profiling of Mg Doped and Undoped GaN

Sample ID	Mg (cm^{-3})	H (cm^{-3})	O (cm^{-3})	C (cm^{-3})
GaN:5	8e19	2.2e20	7.3e19	<2.3e18
GaN:6	4e19	8e19	1.3e19	<1.2e18
GaN:7	------	4e17	1.1e17	1.3e17

As expected, the Mg concentration differed by a factor of two, corresponding to the reduction in Cp_2Mg flow into the reactor. Within the limits of error, the hydrogen concentration differed by approximately the same factor as the Mg. The changes in the C level are unclear due to the lack of sufficient dynamic range in the C signal during measurement. Notably, however, the O level changed by a factor of 5. Theoretical calculations [8] as well as ion implantation [25] have suggested that oxygen is a shallow donor. Zolper *et al.* [25] measured the activation energy of oxygen in GaN to be 29 meV; however, he suggested the possible presence of a deeper oxygen state associated with an oxygen complex. This second deeper oxygen complex state would account for the low activation of his implanted oxygen species as well as a state having a 335 meV activation energy in his unimplanted GaN. Coupling the results of Zolper *et al.* results with the previously noted 5-fold increased in PL intensity of the 2.88 eV transition and corresponding 5-fold increase in the oxygen concentration for samples having a factor of two higher Mg concentration suggests that an oxygen complex participates as the donor in this DA transition.

In light of this conclusion, additions of aluminum which are a possible source of additional oxygen may promote this compensation mechanism in $Al_xGa_{1-x}N$. Hence, increasing Al transport into the reactor may increase the amount of compensation present in Mg-doped $Al_xGa_{1-x}N$ films. Further investigation is needed to confirm or deny this hypothesis. Hall measurements are underway to quantify the free hole concentration, mobility and Mg acceptor level of these films. Tanaka *et al.* [28] reported that for $Al_{0.08}Ga_{0.12}N$ the Mg acceptor state was located 35 meV deeper than that of GaN.

Finally, a $Al_{0.03}Ga_{0.97}N$ p-n homojunction was fabricated. CV measurements clearly indicated the formation of a p-n structure. This was confirmed by the opposite charging effects seen in cross-sectional SEM. The diode characteristics will be reported at a later date.

D. Conclusions

Donor doping of $Al_xGa_{1-x}N$ for $x \leq 0.42$ has been achieved for films deposited at 1100°C. Si-doped $Al_{0.08}Ga_{0.92}N$ and $Al_{0.42}Ga_{0.58}N$ exhibited mobilities of 110 and 14 $cm^2/V{\cdot}s$ at

carrier concentrations of 9.6e18 and 5.0e17 cm^{-3}, respectively. Reasons for these marked changes in electrical behavior include: (1) increased alloy scattering, (2) donor level movement deeper into the gap and (3) donor complex (DX) center type behavior. Acceptor doping of $Al_xGa_{1-x}N$ for $x \leq 0.08$ was also achieved for films deposited at 1050°C. Capacitance-Voltage measurements at 10^4 Hz revealed an activated Mg concentration in the range of 1.5e18 (x=0.08) to 1.5e19 (x=0.03) cm^{-3}. In general, it was found that it was necessary to lower the Cp_2Mg flow rate as the aluminum concentration increased. Based on SIMS profiling of GaN, an oxygen-related state is proposed as the donor which participates in the commonly observed donor-acceptor transitions in Mg doped GaN. Additionally, oxygen incorporation from the aluminum alkyls is potentially responsible for the limited p-type doping of $Al_xGa_{1-x}N$.

E. References

1. S. Strite and H. Morkoc, J. Vac. Sci. Technol. B **10**, 1237 (1992).
2. V. A. Dmitriev, K. Irvine, C. H. Carter, Jr., A. S. Zubrilov, D.V. Tsvetkov, Appl. Phys. Lett. **67**, 115 (1995).
3. B. W. Lim, Q. C. Chen, J. Y. Yang and M. A. Khan, Appl. Phys. Lett. **68** 3761 (1996).
4. M. A. Khan, Q. Chen, C. J. Sun, J. W. Yang, M. S. Shur, Mater. Res. Soc. Proc. **395** 913 (1996).
5. S. C. Binari, Electrochem. Soc. Proc. **95-21**, 136 (1995).
6. P. Boguslawski, E. L. Briggs and J. Bernholc, Phys. Rev B **51**, 17255 (1995)
7. T. Mattila and R. M. Nieminen, Phys Rev B. (to be published) (1996).
8. J. Neugebauer and C. G. Van de Walle, Phys. Rev. B **50**, 8067 (1994).
9. D. W. Jenkins, J. D. Dow and M. Tsai, J. Appl. Phys. **72**, 4130 (1992).
10. T. L. Tansley and R.J. Egan, Phys. Rev B **45**, 10942 (1992).
11. F. R. Chien, X.J. Ning, S. Stemmer, P. Pirouz, M.D. Bremser, R.F. Davis, Appl. Phys. Lett. **68**, 2878 (1996).
12. F.A. Ponce, B.S. Krusor, J.S. Major, Jr., W.E. Plano, D.F. Welch, Appl. Phys. Lett. **67**, 410 (1995).
13. C. R. Abartnathy, presented at 189th Meeting of the Electrochemical Society, Los Angeles, CA, 1996 (to be published).
14 Morton International, *Product Guide and Literature Review,* 1992.
15. P. McGraw, EpiChem, Inc. (Private Communication), 1996.
16. T. W. Weeks, Jr., M. D. Bremser, K. S. Ailey, E. P. Carlson, W. G. Perry, R. F. Davis, Appl. Phys. Lett. **67**, 401 (1995).
17. T. W. Weeks, Jr., M. D. Bremser, K. S. Ailey, E. P. Carlson, W. G. Perry, R. F. Davis, J. Mat. Res. **11**, 1011(1996).
18. M. D. Bremser, W. G. Perry, N. V. Edwards, T. Zheleva, N. Parikh, D. E. Aspnes, R. F. Davis, Mater. Res. Soc. Proc. **395**, 195 (1996).
19. M. D. Bremser, W. G. Perry, K. S. Ailey, N. V. Edwards, O. H. Nam, D. E. Aspnes, R. F. Davis, MRS Internet J. Nitride Semicond. Res. **1**, 8 (1996).
20. J. Bernholc, Mater. Res. Soc. Proc. **423**, (1996).
21. D. V. Lang, R. A. Logan and M. Jaros, Phys. Rev. B **19**, 1015 (1979).
22. D. K. Schroder, *Semiconductor Material and Device Characterization*, (John Wiley & Sons, Inc., New York, 1990), p.41-50.
23. H. Amano, M. Kitoh, K. Hiramatsu, I. Akasaki, J. Electrochem. Soc. **137**, 1639 (1990).
24. W. Götz, N. M. Johnson, J. Walker, D. P. Bour, H. Amano, I. Akasaki, Appl. Phys. Lett. **68**, 1829 (1996).

25. J. C. Zolper, R. G. Wilson, S. J. Pearton, R. A. Stall, Appl. Phys. Lett. **68**, 1945 (1996).
26. S. Nakamura, N. Iwasa, M. Senoh and T. Mukai, Jpn. J. Appl. Phys. **31**, 1258 (1992).
27. J. Neugebauer and C. G. Van de Walle, Appl. Phys. Lett. **68**, 1829 (1996).
28. T. Tanka, A. Watanabe, H. Amano, Y. Kobayashi, I. Akasaki, S. Yamazaki and M. Koide, Appl. Phys. Lett. **65**, 593 (1994).

IV. Growth of III-V Nitride Thin Films on α(6H)-SiC(0001) Via Organometallic Vapor Phase Epitaxy

A. Introduction

With recent world-wide research efforts, the III-V nitride compounds have shown their potential for optoelectronic and microelectronic semiconductor device applications. Advancements in film quality and the understanding of materials issues have led to the demonstration and production of high-quality LEDs. High power, high brightness LEDs with emission spectra ranging from yellow to violet have been produced [1-5]. Using a multiple quantum well heterostructure, Nakamura *et al.* have produced high power blue (5 mW) and green (3 mW) LEDs [5,6] which are now commercially available. There has also been progress recently in the development of laser diodes. Nakamura has demonstrated a current-injected laser diodes on sapphire and spinel substrates with operating voltages around 24 V [7,8]. Although progress has been made in both optoelectronic and microelectronic devices, further developments in the understanding of these materials and improvements in device applications are possible. To further investigate and demonstrate the capabilities of these materials, our research group developed and built a novel organometallic vapor phase epitaxy system. Progress made in the growth of GaN and InGaN films will be discussed in this report.

B. Experimental Procedure

An inverted flow rotating disc OMVPE system was used to grow the nitride films. The design and features of the system have been described in detail in a previous report [9]. The reactants used in the film growth were trimethylaluminum (TMA), triethylgallium (TEG), trimethylindium (TMI) and ammonia (NH_3). Silane (SiH_4) diluted in hydrogen was the silicon source for the n-type dopant. Depending on the film being grown, either hydrogen or nitrogen was used as the diluent. Nitrogen was used as the carrier gas for the metalorganic sources. The system was computer-controlled operated using a LabVIEW (National Instruments) control program developed in-house.

The nitride thin films were grown on on-axis Si-face α(6H)-SiC(0001) substrates. The as-received wafers were cleaved into smaller pieces and degreased. The SiC pieces were then dipped into a 10% HF solution for 10 minutes to remove the thermally grown oxide and then blown dry with N_2. The substrates were then mounted on a molybdenum substrate holder and loaded in the system. The reactor chamber was evacuated to less than 1×10^{-5} Torr before initiating growth. The substrate was heated to the deposition temperature in the flowing diluent. The deposition pressure was 45 Torr. The substrate holder was rotated continuously during the deposition process. The temperature of the substrate was measured using an Ircon Ultimax Infrared Thermometer. While the growth temperature was being obtained, the flow of the

carrier gas through the metalorganic bubblers was established using a run/vent configuration. The temperature and pressure of each metalorganic bubbler were independently controlled.

Once the growth temperature was reached, film deposition was started by flowing the metalorganic precursor(s) and NH_3 into the reactor. For all films grown, a high temperature AlN buffer layer was used. Buffer layers of AlN were grown between 1100 and 1150°C for times ranging from 5 to 30 minutes. The TMA flow rate was varied between 3.0 and 8.0 μmol/min. After the growth of the buffer layer, the temperature was adjusted for the next film layer. GaN growth was investigated in the temperature range between 950 and 1050°C. The TEG flow rate was varied between 17.5 and 25 μmol/min. For Si doping, SiH_4 diluted in hydrogen was introduced into the reactor at flow rates varying between 0.15 and 3.75 nmol/min. The InGaN films were grown between 750 and 800°C. The TEG flow rate was varied between 1.4 and 3.8 μmol/min. The TMI flow rate was varied between 20 and 35 μmol/min. The InGaN films were grown exclusively in nitrogen.

The photoluminescence (PL) properties of the films were determined at room temperature and 4.2 K using a 15 mW He-Cd laser (λ=325 nm) as the excitation source. Scanning electron microscopy (SEM) was performed on a JEOL 6400 FE operating at 5 kV. Transmission electron microscopy (TEM) was performed at 200 keV using standard sample preparation techniques. Capacitance-voltage (CV) measurements were taken using a mercury (Hg) probe and a computer-controlled Hewlett-Packard 4284A LCR meter. Contacts for Hall-effect measurements were made using annealed electron-beam deposited Ti/Au.

C. Results and Discussion

GaN Growth. Figure 1 is an SEM micrograph representative of the quality of the surface of the GaN films. On SiC, it has been shown that a deposition of a high temperature, monocrystalline AlN buffer layer is necessary in order to deposit high-quality GaN films [10]. Figures 2 and 3 are TEM micrographs showing the cross-sectional defect structure of the GaN films. The AlN buffer layer has a smooth surface which helps in the deposition of a low defect density GaN layer. Figure 4 is a TEM plan view micrograph of a GaN sample showing the defect concentration in the film. The dislocation density in the film is on the order of 1e9 cm^{-2}, which is approximately one order of magnitude lower than GaN films grown on sapphire [11]. The absent of defects in the GaN shows up in C-V measurements of the material. Undoped films have a measured net ionized carrier concentration (N_d–N_a) less than 1e16 cm^{-3}, measured at 1 MHz. Si doping of GaN has been achieved in the range of 5e16 cm^{-3} to 3e18 cm^{-3}, as measured by C-V at 1 MHz. The Hall-effect mobility for GaN doped at 2e17 cm^{-3} was measured to be 255 cm^2/V-s, at room temperature. Figure 5 is the PL spectra of GaN at 4.2K. The absence of deep levels is indicative of the high quality of the material. The near-band-edge

peak occurs away from the relaxed value for GaN, possibly indicating strain in the film or near band-edge defect levels. The FWHM is 18 meV.

Gallium nitride films were grown in both hydrogen and nitrogen diluents. There appears to be a difference in film quality depending on the diluent used. Electrical properties for undoped films are similar. However, the PL spectra for the GaN films grown in nitrogen are approximately twice as strong as that for hydrogen grown films. Further optimization of the growth parameters may lead to similar PL results for the two diluents. One other difference between the two diluent gases is the growth rate of the films. AlN buffer layers grown in nitrogen grow at approximately 1/4 the rate of those grown in hydrogen. The GaN films grown in nitrogen grow at approximately 0.7 the rate of those grown in hydrogen. The difference in growth rates can be attributed to the metalorganic chemistry. In the presence of hydrogen, the methyl metalorganic species undergoes an assisted decomposition. The ethyl species, however, decomposes through a β-hydride elimination process, which is influenced less by the presence of hydrogen [12].

InGaN Growth. The InGaN nitride films were grown exclusively in nitrogen. Efforts were made to grow InGaN films in hydrogen, however, the same parameters which yielded indium incorporation in a nitrogen diluent produced only GaN films in a hydrogen diluent. This agrees with other experimental observation [13,14]. It is suggested the hydrogen plays a role in the decomposition of the nitride film, especially in indium containing films. Experiments

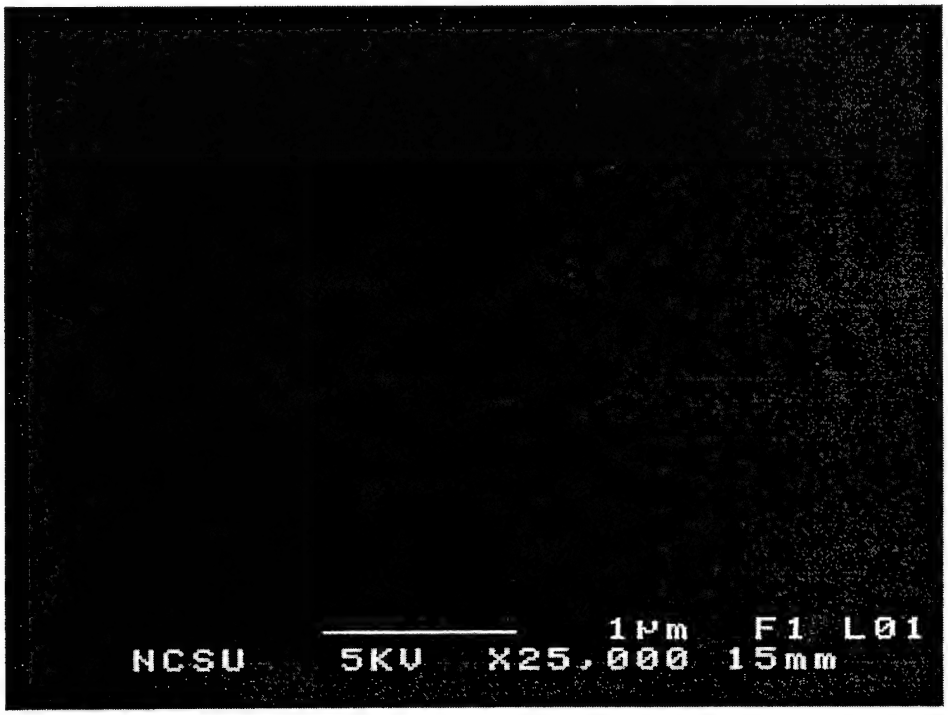

Figure 1. SEM of GaN surface.

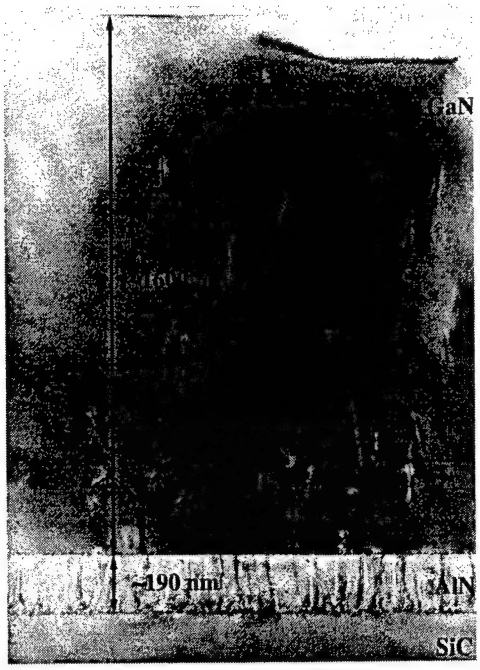

Figure 2. TEM micrograph of GaN and AlN films on SiC.

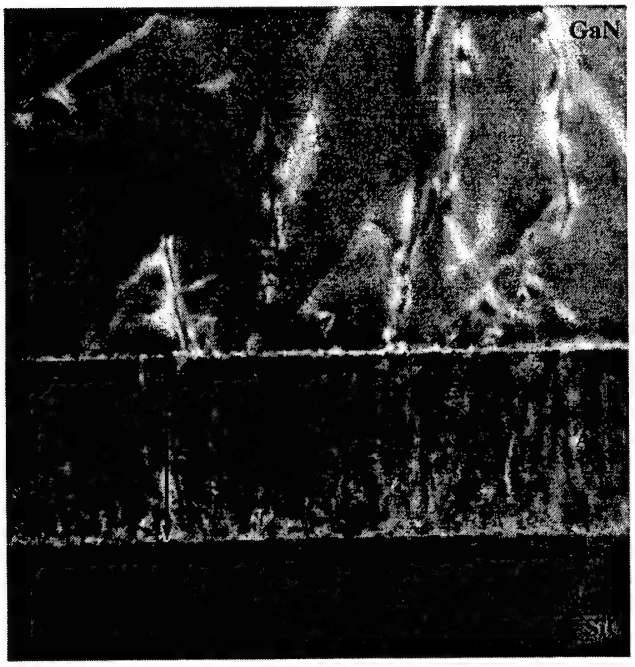

Figure 3. TEM micrograph of GaN and AlN films on SiC.

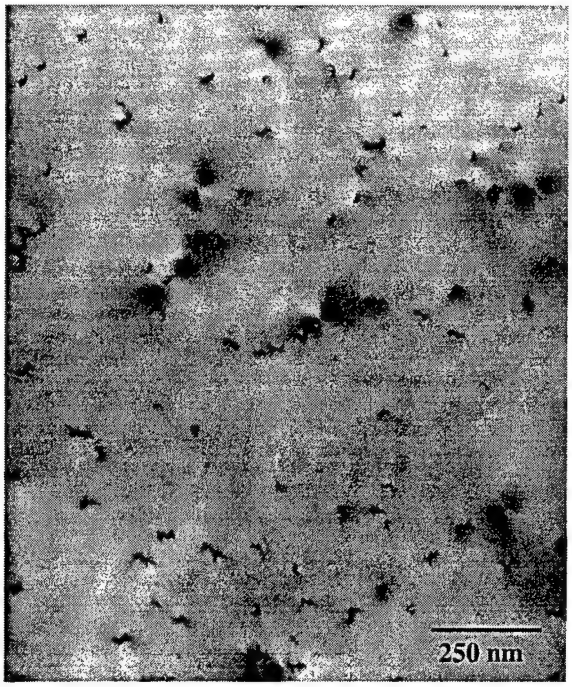

Figure 4. Plan view of GaN film. Dislocation density is approximately 1e9 cm^{-2}.

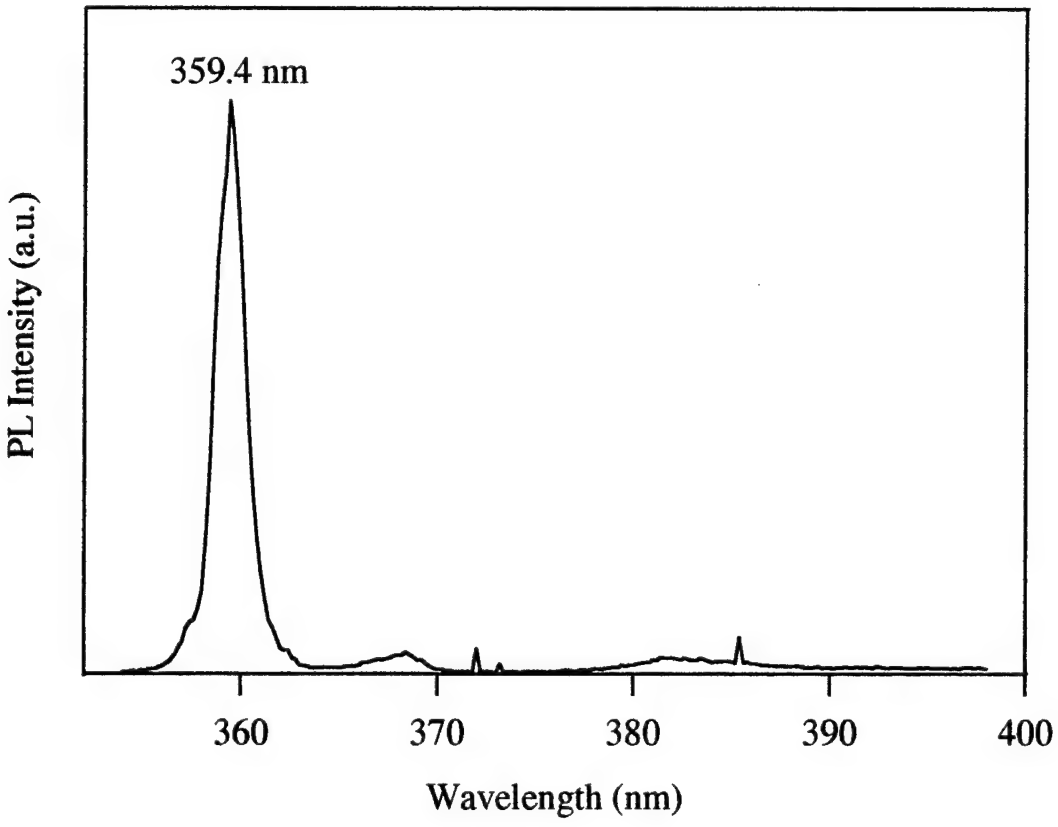

Figure 5. Photoluminescence of GaN at 4.2K.

using helium as a diluent support this argument by duplicating the results obtained using nitrogen diluents, suggesting it is the chemical nature of hydrogen, rather than the diffusion or heat transfer properties of nitrogen, that causes the difference [13].

All of the InGaN films characterized were approximately 1000Å grown on a 5000Å GaN underlayer. $In_xGa_{1-x}N$ films were grown with x as large as 0.22. Figures 6 and 7 are PL spectra for InGaN films at room temperature and 12K, respectively. At room temperature the PL spectra have appreciable deep levels, which disappear at 12K with a noticeable increase in the near-band-edge emission. The emission at 418.5 nm in Figure 6 corresponds to an indium mole fraction of 0.22, while the emission at 405.5 nm corresponds to an indium mole fraction of 0.18 [2]. Figure 8 is a cross sectional TEM micrograph showing the InGaN film on the GaN. The interface is clean, with few threading dislocations generated at the interface. From the TEM, the surface of the InGaN is smooth, however, in SEM small pits can be seen, which may be a result of the surface of the GaN underlayer. With the improvement of the InGaN microstructure, as well as the GaN underlayer, the photoluminescence of the films should improve, providing device-quality material.

D. Conclusions

The growth of GaN and InGaN thin films on α(6H)-SiC(0001) using a high temperature AlN buffer layer has been investigated. SEM and TEM of the GaN films show a smooth surface with a relatively low dislocation density of 1e9 cm^{-2}. The near-band-edge photoluminescence peak occurs away from the relaxed value for GaN, possibly indicating strain in the film or near band-edge defect levels. Si doping of GaN was achieved, with doping levels between 5e16 cm^{-3} and 3e18 cm^{-3}. Gallium nitride growth in hydrogen and nitrogen were compared, with two main differences being photoluminescence intensity and growth rate. InGaN films were grown with an In fraction of up to 0.22. Narrow and bright luminescence was observed both at room temperature and 12K. Cross sectional TEM shows a clean interface between the GaN and InGaN, with few threading dislocations being generated at the interface.

E. Future Research Plans and Goals

Future research includes optimizing the growth of GaN in both hydrogen and nitrogen diluents. p-type doping using Zn and Mg will be investigated. Further research of the InGaN compounds will focus on increasing film quality and the indium mole fraction. Quantum well structures using InGaN active layers will be grown. High speed microelectronic device structures will also be grown and characterized. Finally, quaternary alloys will be investigated in an effort to grow lattice-matched device structures.

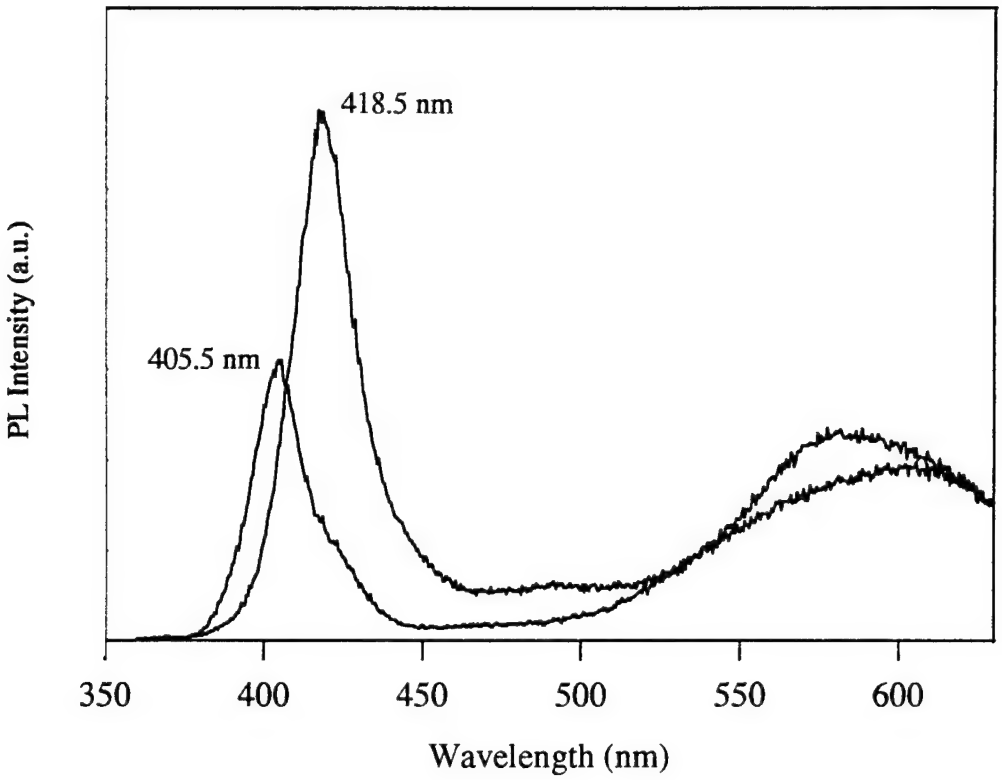

Figure 6. RT PL of $In_xGa_{1-x}N$, x= 0.18 and 0.22 FWHM for x=0.22 is 82 meV.

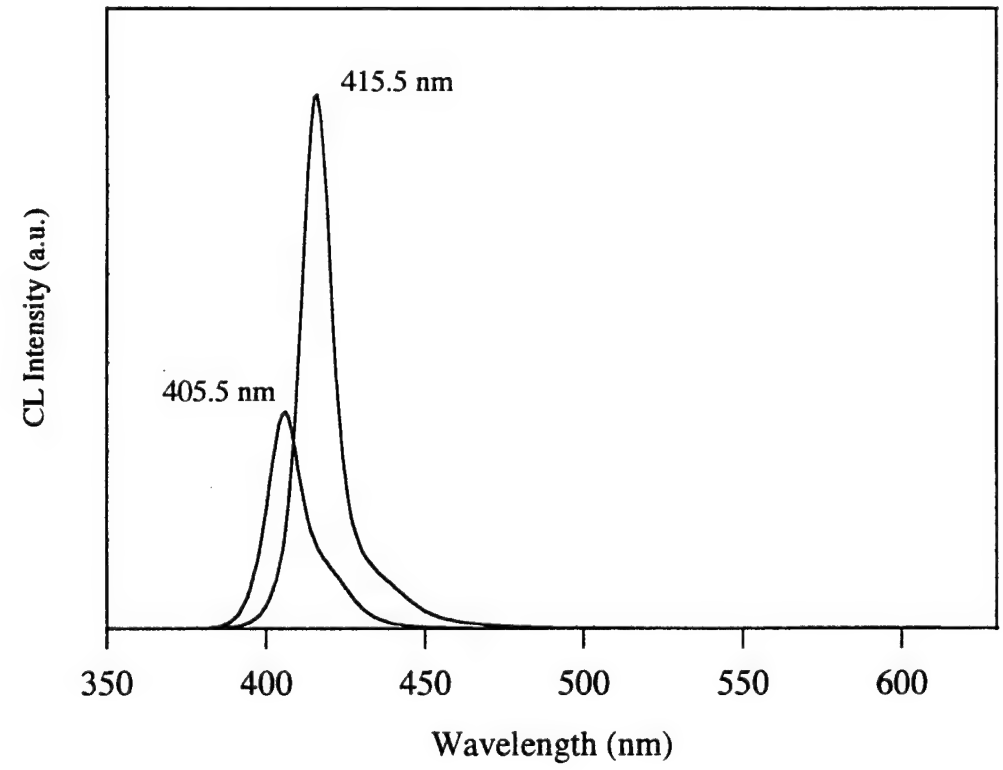

Figure 7. 12K CL of InGaN. x= 0.18 and 0.22.

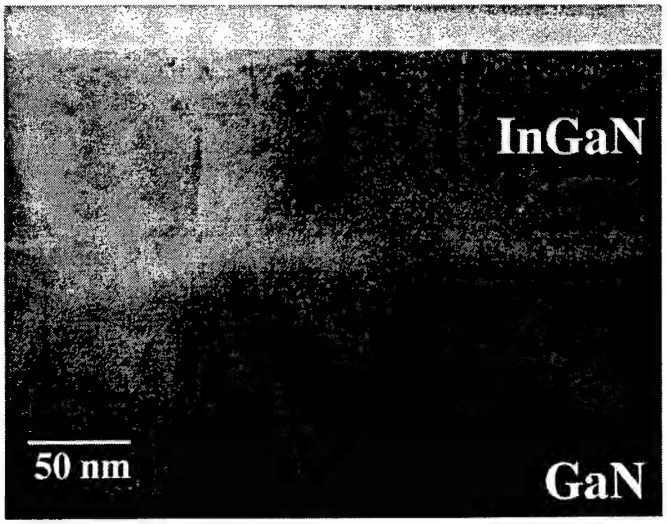

Figure 8. Cross Sectional TEM of $In_{0.22}Ga_{0.78}N$ on GaN.

F. References

1. S. Nakamura, T. Mukai, and M. Senoh, Appl. Phys. Lett. **64** (13), 1687 (1994).
2. S. Nakamura, J. Cryst. Growth **145**, 911 (1994).
3. M. A. Khan, Q. Chen, R. A. Skogman, and J. N. Kuznia, Appl. Phys. Lett. **66** (16), 2046 (1995).
4. S. Nakamura, T. Mukai, and M. Senoh, J. Appl. Phys. **76** (12), 8189 (1994).
5. S. Nakamura, M. Senoh, N. Iwasa and S. Nagahama, Jpn. J. Appl. Phys. **74**, L797 (1995).
6. S. Nakamura, M. Senoh, N. Iwasa, S. Nagahama, T. Yamada and T. Mukai, Jpn. J Appl. Phys. Lett. **34**, L1332 (1995).
7. S. Nakamura, M. Senoh, S. Nagahama, N. Iwasa, T. Yamada, T. Matsushita, H. Kiyoku, and Y Sugimoto, Appl. Phys. Lett. **68**, 2105 (1996).
8. S. Nakamura, M. Senoh, S. Nagahama, N. Iwasa, T. Yamada, T. Matsushita, Y. Sugimoto, and H. Kiyoku, Appl. Phys. Lett. **69**, 1477 (1996).
9. Nitride Semiconductors for Ultraviolet Detection, Semiannual Report, 1994.
10. T. W. Weeks, M. D. Bremser, K. S. Ailey, E. Carlson, W. G. Perry, and R. F. Davis, Appl. Phys. Lett. **67** (3), (1995).
11. W. Qian, M. Skowronski, M. De Graef, K. Doverspike, L. B. Rowland, and D. K. Gaskill, Appl. Phys. Lett. **66** (10), 1252 (1995).
12. K. Jensen, Microelectronics Processing: Chemical Engineering Aspects; American Chemical Society, Washington, DC, (1989).
13. M. Weckwerth, K. Killeen, R. Biefeld, T. Drummond, M. Crawford and J. Zolper, EMC, Santa Barbara, Session CC: Growth and Processing of III-V Nitrides, June 1996.
14. E. Piner, J. Roberts, G. McIntosh. Private Communication.

V. Correlation of Biaxial Strains, Bound Exciton Energies, and Defect Microstructures in GaN Films Grown on AlN/6H-SiC(0001) Substrates

A. Introduction

Mismatches in the lattice parameters (*a* and *c*) and the coefficients of thermal expansion (α) exist between heteroepitaxial GaN films and all of the presently used substrates. These mismatches result in interfacial biaxial strain which leads to misfit dislocations and associated threading defects that degrade film quality. Measurement and analysis of these strains have been the goals of the research reported herein.

The most common substrate used for GaN film growth is sapphire (0001). Buffer layers of AlN and GaN have been used to improve GaN film quality, although significant mismatches in the lattice parameters between these layers and sapphire exist ($\Delta a/a_o \approx$ 13.6 and 16.1%, respectively, see Table I). The resulting lattice mismatch strain is compressive for both GaN on AlN and GaN on sapphire and alters the values of both *a* (decreases) and *c* (increases) of the films [1,2]. Hiramatsu *et al.*[3] have assumed this strain to be relieved after several nanometers of growth according to the critical thickness theory. The primary relief mechanism is the formation of dislocations at the film/substrate interface during film growth. Upon cooling, the difference in thermal expansion coefficients ($\alpha_{sapphire} > \alpha_{AlN} > \alpha_{GaN}$) results in additional compressive stresses which are often assumed [1,4] to be wholly responsible for the observed compressive strain. However, high resolution transmission electron microscopy (HRTEM) analysis of the GaN/AlN interface on sapphire [5] suggests that the lattice mismatch stress in GaN is not fully relieved. This residual stress was assumed [5] to be accommodated elastically and to give rise to biaxial stresses in the GaN films. However, it is difficult to substantiate this through other characterization techniques since both thermal and lattice mismatch stresses are compressive, and there is a marked variation in published thermal expansion coefficients that could be used in calculations. Moreover, none of these coefficients applies to temperatures above 900°C, where most GaN thin films are deposited.

Recent work [6,7] has used a SiC(0001) substrate/AlN(0001) buffer layer combination. The lattice mismatch strains at both the GaN/AlN and AlN/SiC interfaces are compressive ($a_{GaN} > a_{AlN} > a_{SiC}$), but the reduced lattice mismatch between AlN and SiC (~1%) compared to AlN and sapphire leads to improved GaN film quality. This mismatch is expected to be at least partially relieved by the formation of misfit dislocations, as the calculated critical thickness for AlN(0001) on SiC(0001) is only 47Å [8]. The differences in thermal expansion coefficients are opposite in sign ($\alpha_{GaN} > \alpha_{SiC} \approx \alpha_{AlN}$) to that for GaN on sapphire and result in a biaxial tensile stress contribution. Hence, the two main stresses in the GaN/AlN/SiC heteroepitaxial

To be Published: Journal of Electronic Materials, Special III-V Nitrides Edition

system are opposite in sign, which offer the potential to substantiate if residual lattice mismatch stress exists through lattice parameter measurements and other techniques. Li and Ni [9] measured the lattice parameters for thick GaN films grown directly on both SiC(0001) and sapphire(0001). They observed that the film on SiC was in tension while that on sapphire was in compression. They attributed this variation in strain to the difference in thermal expansion coefficients between the two substrates.

Table I. Comparison of III-Nitride Material Properties with 6H-SiC and Sapphire[a].

Material	Lattice Parameter at RT(Å)	In-Plane Mismatch with GaN (%)	Coefficients of Thermal Expansion (10^{-6}/K)
GaN	a=3.1891[b]	---	5.59; 3.1,6.2[d]
	c=5.1855[b]		7.75[c]; 2.8,6.1[d]
AlN	a=3.112	2.5	4.15
	c=4.982		5.27
6H-SiC	a=3.08	3.5	4.2; 3.2,4.2[d]
	c=15.12		4.68; 3.2,4.0[d]
Sapphire	a=4.758	16.1	7.5; 4.3,9.2[d]
	c=12.99		8.5; 3.9,9.3[d]

[a] *Landolt-Börnstein*, edited by O. Madelung (Springer, New York, 1982), Vol. 17.
[b] C. M. Balkas, C. Basceri, and R. F. Davis, Powder Diffraction **10** 266 (1995).
[c] *Properties of Group III Nitrides*, edited by J. H. Edgar (INSPEC, London, 1994).
[d] M. Leszczynski, T. Suski, P. Perlin, H. Teisseyre, I. Grzegory, M. Bockowski, J. Jun, S. Porowski, J. Major, J. Phys. D: Appl. Phys. **28** A149 (1995), For T =300-350 K and 700-750 K, respectively.

One consequence of film strain is a shift in the band-gap energy (E_g) [10]. The biaxial strain can be viewed as an isotropic cubic component together with a uniaxial component along the c-axis of the GaN film [11]. The cubic, or hydrostatic term influences the band gap directly, while the uniaxial component introduces subtle shifts between individual lines in the spectrum. However, it is difficult to measure E_g directly in GaN due the strong excitonic features at the absorption edge [12]. Changes in E_g may be detected by shifts in these excitonic features using low temperature photoluminescence (PL). At $T \leq 4.2$ K the PL of high-quality GaN reveals intense near-band edge emission attributed to the recombination of both free excitons and/or excitons bound to shallow neutral donors [4,6,7,12,13]. The bound exciton feature is often the dominant feature due to the nature of GaN, which is always n-type for undoped films. The identity of the shallow donor(s) is unknown, although recent work suggests that both native defects and extrinsic impurities are possibilities [14-16]. Amano, *et al.* [1] observed a shift of the bound exciton energy (E_{BX}) to higher energies that was attributed to biaxial compressive

strain for GaN films deposited on sapphire(0001). Reported E_{BX} values range from 3.467 to 3.494 eV for GaN on sapphire [12,13,17,18], and from 3.463 to 3.472 for GaN on SiC [4,6,7,18,19]. The disparity between the two energy ranges has been attributed to the difference in thermal expansion coefficients of the two substrates [4,18].

In this research, the relationship between E_{BX} and lattice parameters (and hence strain) was determined for 22 GaN films grown on AlN buffer layers previously deposited on 6H-SiC(0001). A value of E_{BX} for relaxed GaN was determined. Poisson's ratio was calculated from lattice parameter measurements and used to determine the shift of E_{BX} with biaxial stress (σ_a). The roles of the AlN buffer layer and the tilt of the SiC substrate on film stress and the associated PL spectra were also determined. Transmission electron microscopy (TEM) was employed to compare and contrast the crystal structure of GaN films grown on the vicinal (off-axis) and on-axis SiC wafers. The GaN/AlN interface was analyzed via high resolution (HR)TEM to determine if any residual lattice mismatch stress occurred.

B. Experimental Procedures

The GaN/AlN films were grown in an organometallic vapor phase epitaxial (OMVPE) system described previously [6,7] on both on-axis and vicinal (2-4° off-axis) 6H-SiC(0001) substrates. The GaN films ranged in thickness from 0.3-3.7 μm and were grown at temperatures ranging from 950-1100°C. The AlN buffer layer for each sample was 1000 Å thick and grown at 1100°C. All of the GaN films were unintentionally doped, with *n*-type carrier concentrations ranging from $<1\times10^{16}$–$1\times10^{17}/cm^3$.

Absolute lattice constants values were measured using a Philips X'Pert MRD X-ray diffractometer in the triple-axis mode. The technique used was originally proposed by Fewster [20], and is comparable to, and in many ways more accurate than, the commonly used "Bond" method. The high resolution of the triple-bounce analyzer crystal and the steps taken to eliminate inaccuracies due to the 2θ zero error and sample centering account for this. The data were collected using 2θ-ω scans, with corrections made for refraction. The accuracy of the lattice parameters measured using this system was 0.0002Å. The c-axis lattice parameter (*c*) was measured using the (002) reflection. Measurements of the a-axis lattice parameter (*a*) were made using both the (002) and (015) reflections; however, the low count rate for the asymmetric reflections limited the number of samples that could be measured accurately.

Photoluminescence (PL) measurements of the GaN films on SiC were made at 4.2 K using a He-Cd laser (λ=325 nm) as the excitation source, unless otherwise noted. TEM studies were performed using a TOPCON EM - 002B HRTEM, operated at 200 kV with a point-to-point resolution of 0.18 nm. The cross-sectional samples in the $[11\bar{2}0]$ orientation were prepared by conventional techniques using mechanical grinding and polishing, and Ar^+ ion-milling at a low angle in the final stage [21, 22].

PL/XRD Analysis. Low temperature PL of the GaN(0001) films grown in this research exhibited strong near-band-edge emission due to the recombination of both free and donor-bound excitons, as shown in the spectrum from a 3.7 μm thick film in Fig. 1. The emission from the donor-bound exciton (BX) decreased in intensity much faster than that from the free excitons (FX) as the temperature was increased from 10 to 100 K. This behavior is due to the small localization energy (E_b) of the donor-bound excitons compared to the binding energy of the free excitons (E_x). From this data E_b was estimated to be 5.9 meV, which agrees favorably with earlier measurements [7,13]. Recent work on this and other samples measured E_x to be 21±1 meV for the A- and B-free excitons [23], although earlier work suggested a higher (26 meV) value [13]. The PL of the GaN films in this study was dominated by the bound exciton emission, and its dependence on lattice strain as manifest in changes in lattice parameters will be described below.

The bound exciton energies (E_{BX}) determined at 4.2 K as a function of the c-axis lattice parameter (*c*) for 22 GaN films on SiC are shown in Fig. 2. The lattice parameter measurements measurements were performed at room temperature. It is expected that the tensile strain in the

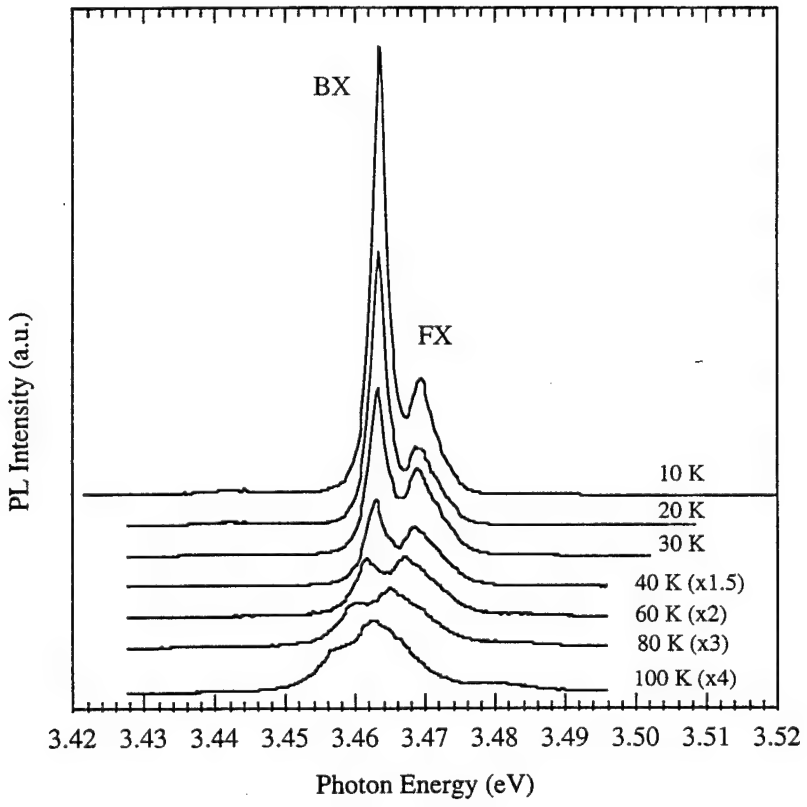

Figure 1. PL of a 3.7 μm thick GaN film on an AlN buffer layer previously grown on a SiC(0001) wafer at 10, 20, 30, 40, 60, 80 and 100 K. The peaks labeled BX and FX are due to the recombination of bound and free excitons, respectively.

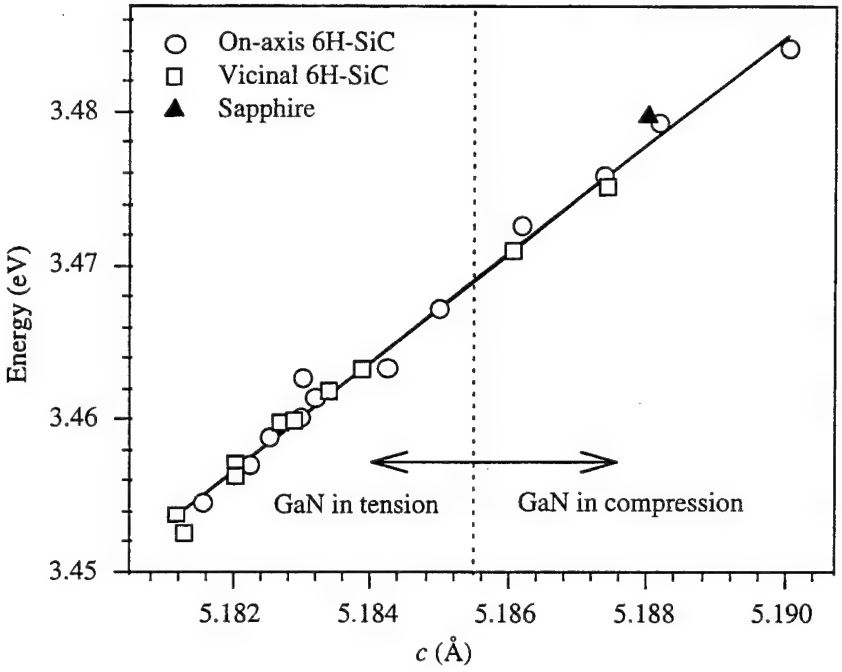

Figure 2. Lattice constant c vs. the bound exciton energy (E_{BX}) for GaN/AlN/SiC. The PL was performed at 4.2 K and the lattice parameter measurements at room temperature. The dashed line indicates the relaxed value of C_o (5.1855 Å) for GaN. A data point for GaN grown on sapphire is included.

GaN films due to thermal expansion mismatch will increase as the temperature is decreased from room temperature to 4.2 K, but lattice parameter measurements are not possible at these temperatures. A linear relationship between the c and E_{BX} was observed, where the bound exciton peak shifted to lower energies as c decreased. Any change in c is in response to a strain (ε_a) along the a-axis (a), $\Delta a/a_o$, which results from the biaxial stress produced in the plane of the film by residual stresses. Thus a decrease in the value of c indicates that the biaxial tensile strain in the film is increasing, which causes E_g to decrease and E_{BX} to shift to lower energies.

The value of c for relaxed GaN has recently been measured to be 5.1855 Å [24]. As shown in Fig. 2, six of the GaN films grown on SiC(0001) have values of c greater than this, which indicates they are compressively strained. This suggests that the compressive strain due to lattice mismatch has not been fully relieved by defect formation in these samples. The highest value of c observed was 5.190 Å, and the bound exciton energy for this sample was 3.484 eV. The highest reported E_{BX} value previously reported for GaN grown on 6H-SiC was 3.472 eV [19]. The n-type carrier concentration of this film was reported to be 1×10^{18} cm^{-3}; thus it is possible that this value was slightly shifted to higher energies by the Burstein-Moss [25] effect rather than by strain. The free carrier concentration for the samples in this study was less than 1×10^{17}/cm^{-3}; therefore, it is assumed that the shift observed in E_{BX} in this study was not due to this effect.

Values of E_{BX} can be estimated from a linear regression of the data in Fig 2, which yielded $E_{BX} = (-14.91 + 3.545*c)$ eV, where c is in angstroms. Using this relationship E_{BXo} was predicted to be 3.469 eV for relaxed GaN. This compares favorably to reported values of 3.467, [26] 3.469, [27] and 3.472 eV[28]. The marked dependence of the values of E_{BX} on c indicated that the wide range of energy values reported for the donor-bound exciton in the literature are due primarily to different amounts of strain present in the films. For GaN on sapphire, typical E_{BX} values are between 3.467-3.494 eV, which are predominantly in the energy range indicated for films under compression in this study. Included in Fig. 2 is a data point for a 4.7 μm GaN film grown on sapphire, which indicated that E_{BX} can be predicted for GaN grown on any substrate using values of c and the relationship determined in this study.

For biaxially strained wurtzitic films the relationship between the lattice parameters c and a is given by the strain ratio [29],

$$\varepsilon_c/\varepsilon_a = (\Delta c/c_o)/(\Delta a/a_o) = -2\upsilon/(1-\upsilon), \quad (1)$$

where υ is Poisson's ratio and a_o and c_o are the relaxed lattice parameters. For GaN, values of υ which range from 0.372 [30] to 0.20 [31] have been calculated using anisotropic elastic constants. A recent survey [32] of x-ray data available in the literature determined $\upsilon = 0.23 \pm 0.06$ for samples dominated by biaxial strain. In this study a and c were measured simultaneously for 22 GaN films on 6H-SiC, including 10 of those shown in Fig. 2. The relationship between a and c is displayed in Fig. 3. Also included is a data point for the 4.2 μm GaN film on sapphire included in Fig. 2. An average strain ratio of $\varepsilon_c/\varepsilon_a = -0.455$ was determined for this data set using values of 3.1891 Å and 5.1855 Å for a_o and c_o, respectively [28], which resulted in a Poisson's ratio of $\upsilon = 0.18$. Further analysis showed that remarkably different strain ratios of $\varepsilon_c/\varepsilon_a = -0.33$, -0.47, and -0.59 were calculated from the same data using other published values for a_o and c_o.[32,2,33] This disparity in the strain ratios was due to individual values of c and a that were close to the different values for a_o and c_o which resulted in abnormal values in the nominator and/or denominator of equation (1) for that sample's strain ratio. A distortion of the average strain ratio for the data set resulted.

Given this wide variation in the calculated strain ratios two methods were used to obtain a more reasonable estimation of the strain ratio and the resulting Poisson's ratio. The first eliminated those data points (4 total) that had adverse effects on the average strain ratio of the data set. An average strain ratio was then calculated using each of the four sets of published values for a_o and c_o [28,32,2,33] and averaged to give a strain ratio $\varepsilon_c/\varepsilon_a = -0.425$. The corresponding Poisson's ratio was $\nu = 0.18$. The second method fit a line to the data in Fig. 4, and then used the experimentally determined values of c to calculate values of a that fit the line. The strain ratio for each point was then calculated using values of $c_o = 5.1850$ and $a_o = 3.1891$,

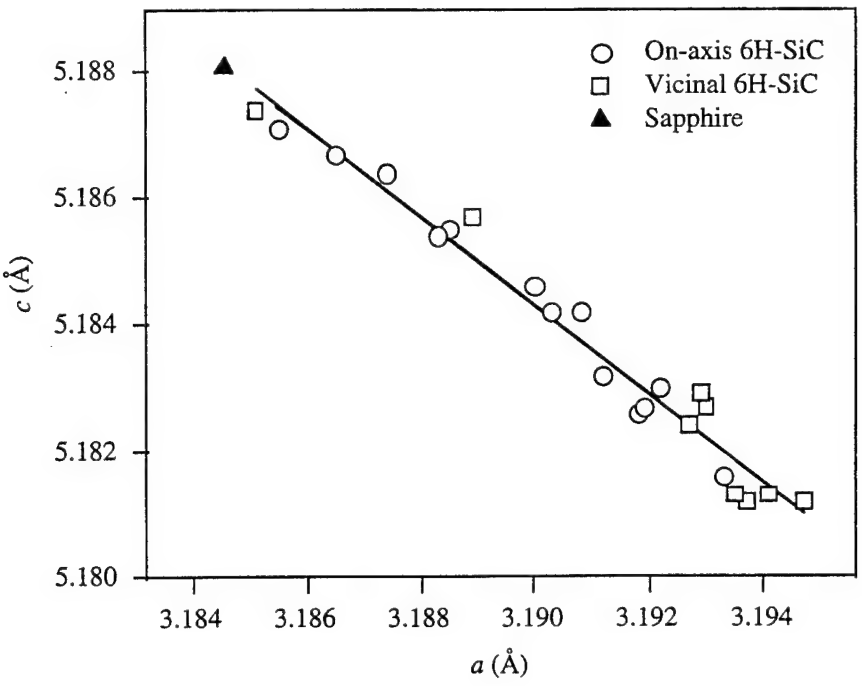

Figure 3. Lattice constant α vs. *c* for GaN/AlN/SiC. The lattice parameter measurements were performed at room temperature. The Poisson's ratio calculated using this data as $\nu = 0.18 \pm .02$.

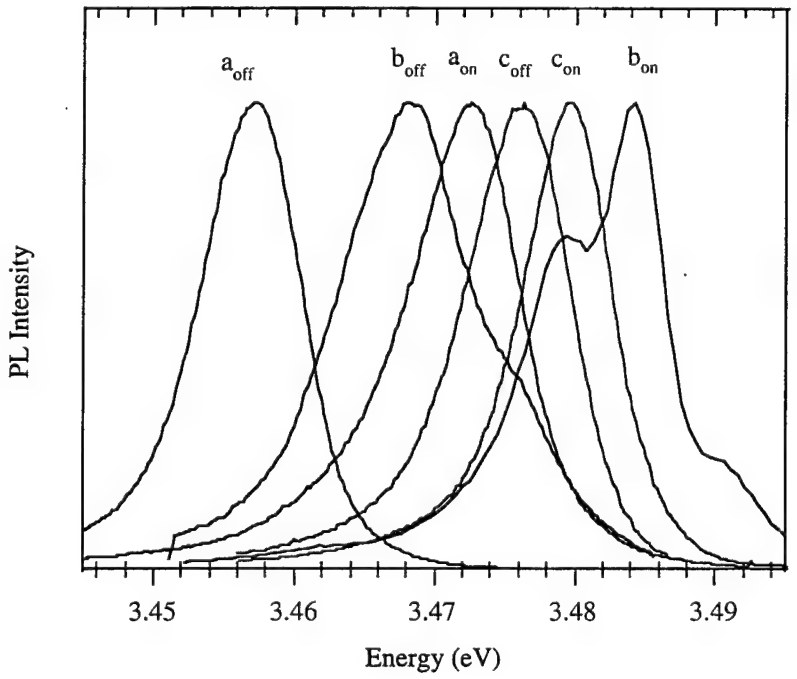

Figure 4. PL at 4.2 K of three sets of GaN films (a, b, c) grown concurrently on vicinal (off-axis) and on-axis SiC. The off-axis tilt of sample *c* is ~2°, which is lower than a tilt of 3–4° that is typical for the vicinal wafers.

where the latter value was determined from the line fit to the data in Fig. 4. The average strain ratio using this method was $\varepsilon_c/\varepsilon_a = -0.446 \pm .03$, which resulted in a Poisson's ratio of $\upsilon = 0.18 \pm .02$. The two calculated values of Poisson's ratio were identical, and they compared favorably with values determined from x-ray data ($0.23 \pm .06$ [32]) and anisotropic elastic constants (0.20 [31], 0.24 [34] and 0.26 [35]).

The shift of E_{BX} as a function of the biaxial film stress ($\Delta E_{BX}/\Delta\sigma_a$) can be estimated from the data in Fig. 2 using the relationship [29],

$$\sigma_a = Y/(1-\nu)\varepsilon_a = -Y\varepsilon_c/2\nu, \qquad (2)$$

where Y is the Young's modulus (290 ± 20 GPa).[32] The first step was to calculate $\Delta E_{BX}/\Delta\varepsilon_c$ from the data in Fig. 2, where relaxed values of $E_{BXo} = 3.469$ eV and $c_o = 5.1855$ Å were assumed. A linear regression of the data yielded $\Delta E_{BX}/\Delta\varepsilon_c = 18.1$ eV. Using this expression, and the previously determined Poisson's ratio of $\nu = 0.18$, a value of $dE_{BX}/d\sigma_\alpha = 23$ meV/GPa was calculated. This result is lower than that reported previously for hydrostatic pressure experiments (39 [36] and 40 [37] meV/GPa), but it compared favorably to results for GaN films where biaxial stress was assumed 27 [32,38] meV/GPa). However, the similarity of the value given in Ref. [38] with that determined in this research may be a coincidence given that the authors assumed the wrong relationship between stress and strain. It should be noted that uncertainties in Poisson's ratio and Young's Modulus can have a dramatic effect on these calculations.

The role of SiC off-axis tilt on GaN film stress was investigated using films grown concurrently on off- and on-axis SiC(0001) wafers. Previous analysis in this laboratory of 1.4 μm GaN/AlN films deposited simultaneously on vicinal and on-axis 6H-SiC(0001) substrates showed the microstructural quality of the GaN and AlN layers on the on-axis substrate to be superior [7]. Moreover, double crystal x-ray curve (DCXRC) measurements showed a FWHM of 58 arcsec for the on-axis film, compared to 151 arcsec for the vicinal film. Plan view TEM measurements showed a lower dislocation density for a GaN film on the on-axis SiC, and the AlN buffer layer was of high microstructural quality. The bound exciton energy of the vicinal film was shifted to a lower energy relative to the on-axis film, with $\Delta E_{BX} = 3$ meV.

The PL spectra of the bound exciton emission from three separate GaN film sets grown concurrently on off- and on-axis SiC are displayed in Fig. 4, where the film thickness was ≤ 0.6 μm for all of the samples. In each case the BX emission on the vicinal wafers was shifted to lower energies, with ΔE_{BX} as large as 17 meV. A related shift in the lattice parameter c was observed, with Δc as great as 0.0072 Å. Thus the GaN films grown on vicinal SiC were compressively strained compared to those grown on on-axis SiC. The disparity in E_{BX} and c values persisted as the film thickness increased. However, ΔE_{BX} decreased, and E_{BX} for both

types of films shifted to energies commonly associated with GaN on 6H-SiC(0001) ($E_{BX} \geq 3.469$ eV). It should be noted that the values of *c* for the underlying vicinal and on-axis 6H-SiC were identical at the AlN/SiC interface, which indicated that the phenomena discussed is not due to differences in the lattice constants of the substrates.

TEM/HRTEM Analysis. To understand these results it is necessary to examine the defect microstructures of GaN films grown on an AlN buffer on 6H-SiC(0001) substrates. The primary defects in the AlN buffer layers grown on the off-axis SiC substrates were domains and their associated domain boundaries, as shown by HRTEM in Fig. 5 and lower magnification TEM in Figs. 6(a) and (b). Recent studies [39] show that the steps on the vicinal surface provide sites for the growth of inversion domains, which are separated by inversion domain boundaries (IDBs). These defects introduce a marked amount of strain in the AlN buffer layer grown on off-axis SiC substrate. There is also a high density of threading dislocations in the buffer layer.

By comparison, the crystal quality of AlN films grown on on-axis SiC substrate is of improved crystalline quality, as shown by HRTEM in Fig. 7 and TEM in Fig. 8. Most significantly, there is a reduced density of inversion domain boundaries due to the reduction in the density of SiC steps. The primary defects are stacking faults parallel to the AlN/SiC interface and associated partial dislocations. Threading dislocations running from the top to the bottom of the film are also present.

The crystal quality of the GaN is directly influenced by the AlN buffer. The inferior quality of the AlN buffer layer grown on vicinal SiC results in a high dislocation density ($\sim 10^9$–$10^{10}/cm^2$) at the interface, as determined from plan-view TEM analysis by counting the number of dislocations per unit area. The dislocation density decreases markedly about two hundred angstroms away from the GaN/AlN interface. The predominant defects are threading dislocations and threading segments that persist throughout the film. In addition stacking faults and dislocation loops are observed close to the interface. Finally, domain boundaries that originate at the GaN/AlN interface are also visible. It should be noted though that recent work has shown that the formation of domains can also be associated with non-stoichiometry or contamination of the AlN surface [40].

The improved quality of the AlN buffer layers on the on-axis SiC carries over into the GaN, as displayed in Fig. 8. A dislocation density in the order of $\sim 10^8/cm^2$ in the GaN layer was observed in plan-view TEM near the GaN/AlN interface. Most notably there are no planar defects such as stacking faults or domain boundaries in the GaN. The dominant defect in the on-axis GaN films are edge-type dislocations with burgers vectors $\mathbf{b} = 1/3\langle 11\bar{2}0\rangle$ and $\mathbf{b} = 1/3\langle 1\text{-}100\rangle$. These are the misfit dislocations which form at the GaN/AlN interface. This TEM anslysis, as well as that of other [41] NCSU samples, reveal that the lattice mismatch

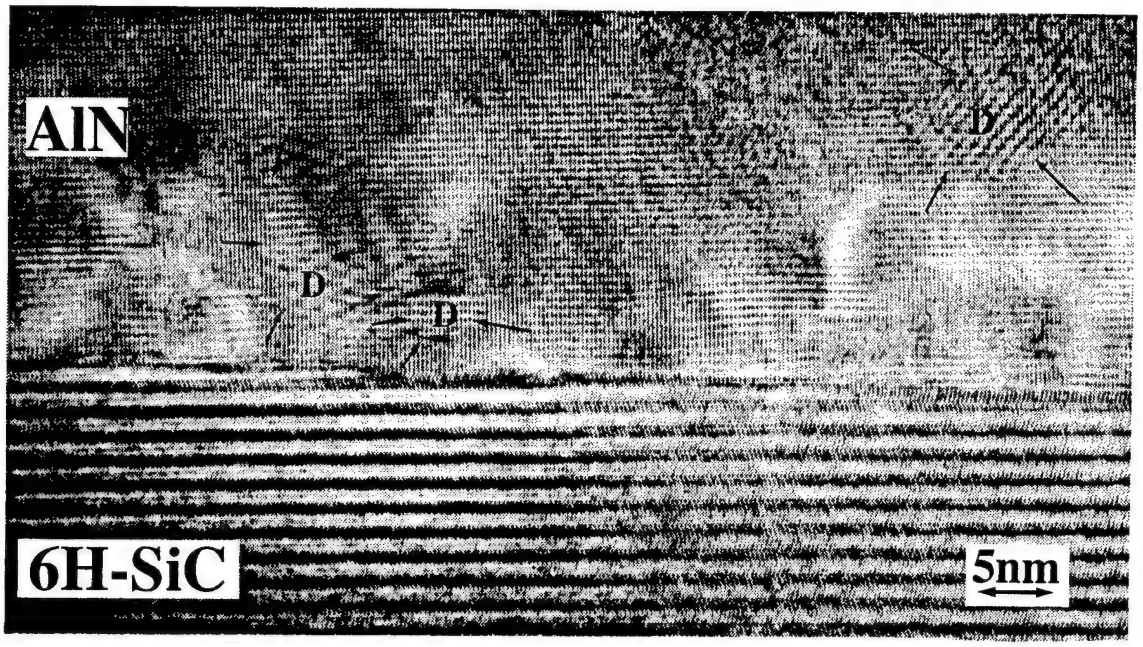

Figure 5. HR micrograph from an AlN/6H-SiC vicinal interface reveals that the strain at the interface is due to the numerous domain boundaries (denoted by D and the arrows) formed when neighboring grains coalesce during the growth process.

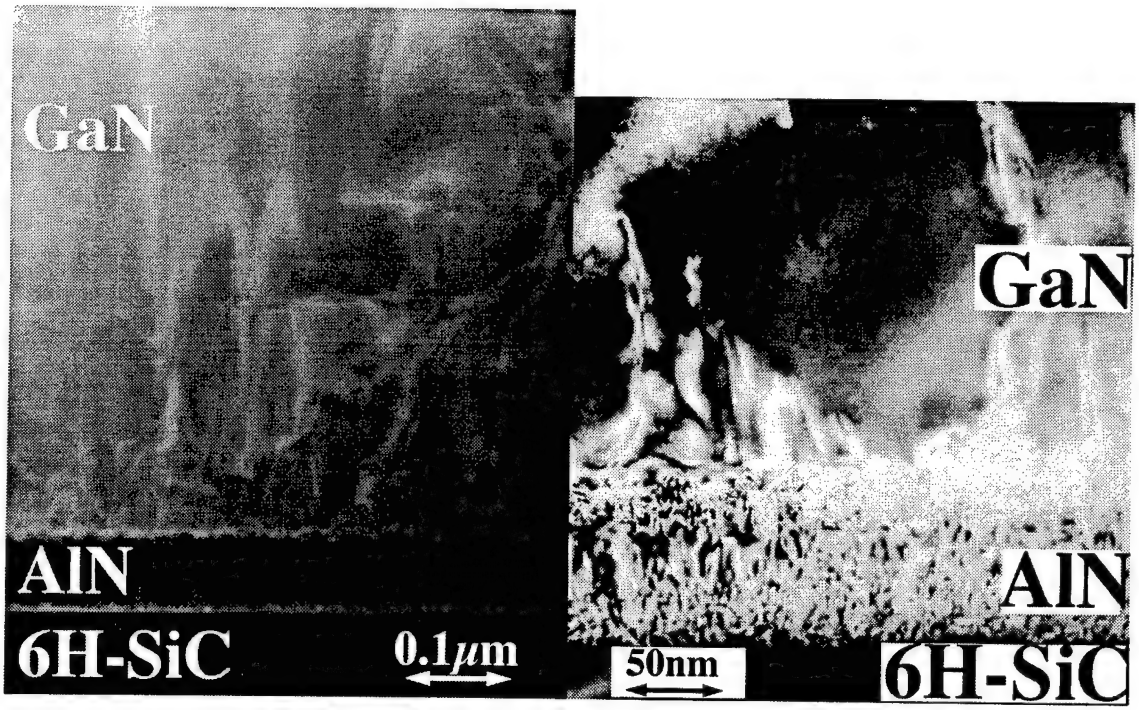

(a) (b)

Figure 6. Low magnification TEM micrographs of a GaN/AlN/vicinal 6H-SiC(0001) heterostructure. (a) the AlN film exhibits domain type of growth with characteristic domain boundaries. Plan view of the GaN film reveals a dislocation density of ~10^{10}-10^{11}/cm^2 comprised mostly of threading dislocations and threading segments. (b) The nonuniform contrast in the AlN film is due to the overlapping stress fields at the AlN/6H-SiC and GaN/AlN interfaces from the lattice parameters and coefficients of thermal expansion.

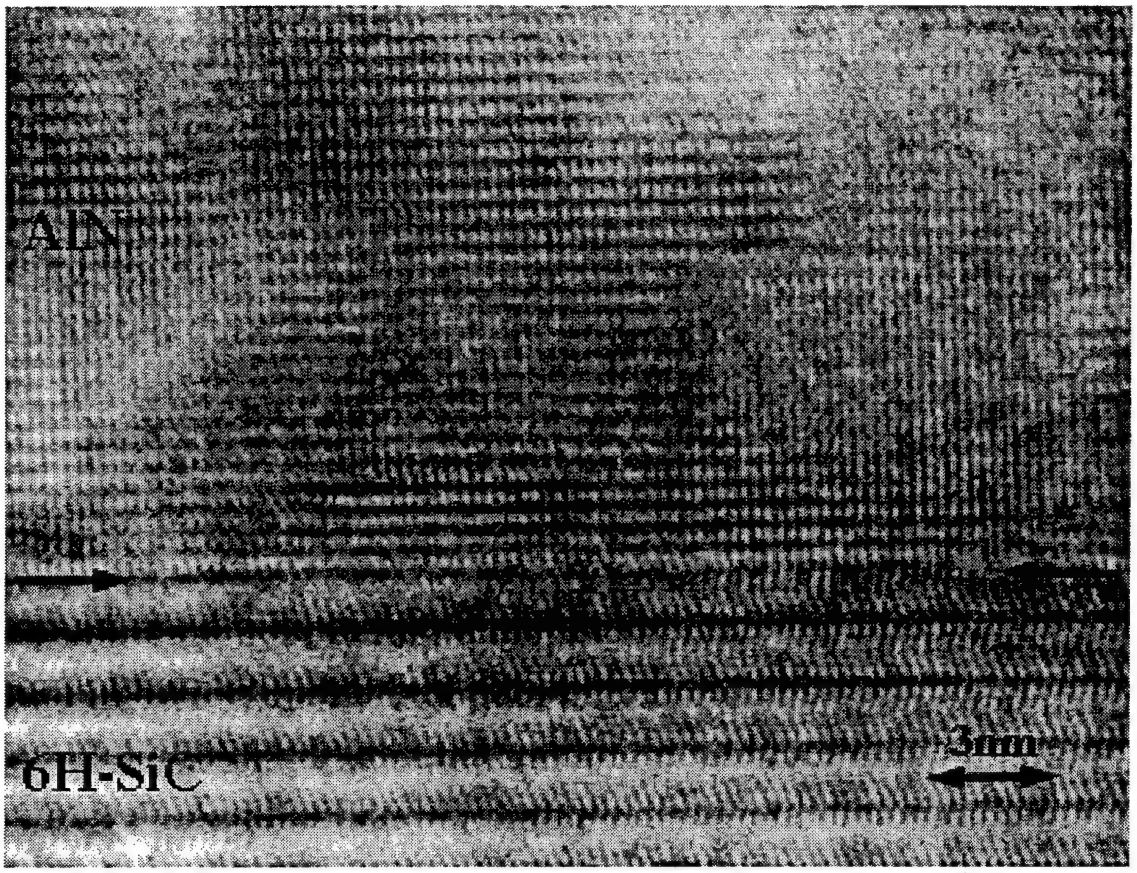

Figure 7. HRTEM micrograph from AlN on on-axis 6H-SiC(0001). There are no domains and associated domain boundaries as observed in the off-axis films shown in Fig. 5.

stress in GaN films grown on the on-axis SiC substrate is accommodated mostly by misfit dislocations. However, our PL, XRD and TEM studies suggest that these defects do not provide full stress relief.

In order to further assess the residual strain in the GaN films, HRTEM studies were performed at the GaN/AlN interface of the on-axis SiC in the [11$\bar{2}$0] orientation, as shown in Fig. 9. It can be seen that the interface is epitaxial and free of domains, threading dislocations and low angle grain boundaries. Using HRTEM, it is possible to calculate the residual strain at the interface for planes that are perpendicular to the interface and parallel to each other. Ning, *et al.* [5], used this method to calculate the misfit at the GaN/sapphire interface, where they found a ~1% residual strain in the GaN film.

To determine the residual strain in the GaN films grown in the present research, the average lattice mismatch was calculated along the GaN/AlN interface from HRTEM micrographs in [11$\bar{2}$0] GaN orientation, by counting the number of (1-100) GaN and AlN planes along [1-100] direction that was bounded on each end by commensurate GaN and AlN planes. The

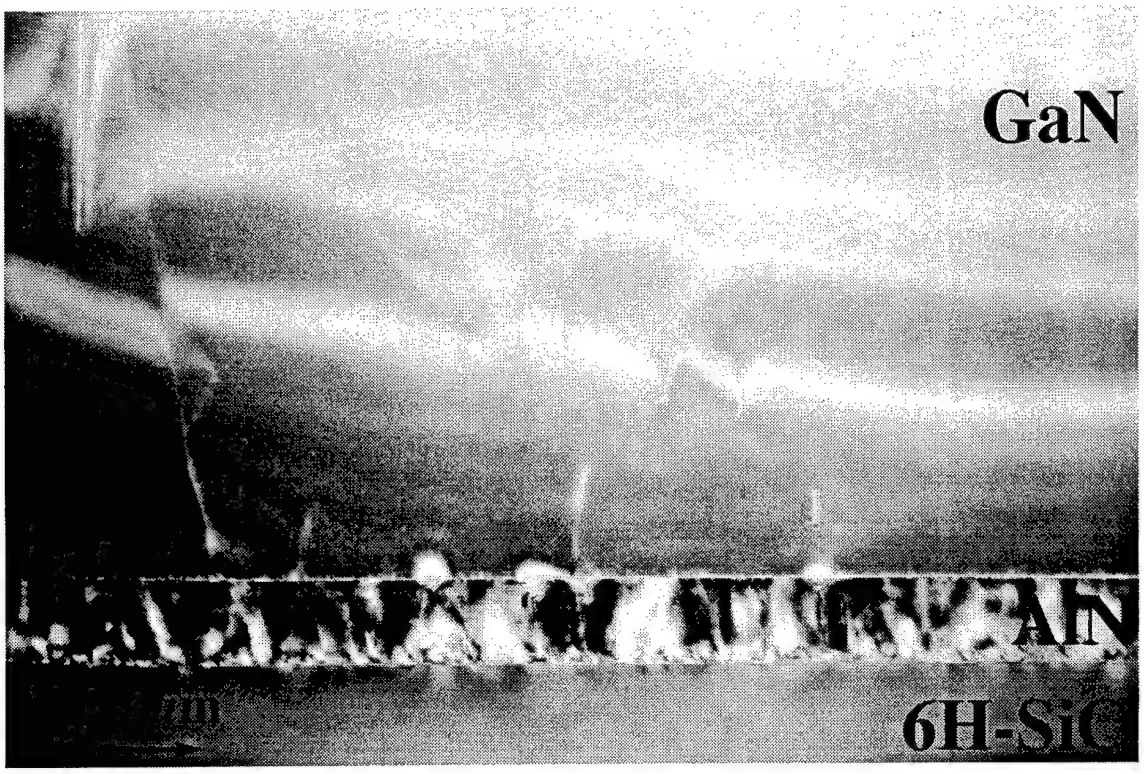

Figure 8. TEM micrograph from the GaN/AlN/on-axis 6H-SiC(0001) heterostructure in [11$\bar{2}$0] orientation showing the considerably improved quality of the GaN/AlN and AlN/SiC interfaces relative to those achieved with the vicinal substrate (see Fig. 6a). Note also the reduction of the defect density in comparison with the structure grown on the off-axis SiC substrate.

experimental mismatch was assessed to be 0.9% lower than the theoretical misfit value of 2.5% for GaN and AlN. The experimental mismatch is equal to $N_{GaN} - N_{AlN}/N_{AlN}$, where N is the number of (1-100) planes perpendicular to the interface (Fig. 9). This calculation was repeated at ~20 different locations along the interface, with the average results presented here. Thus, there is a 0.9% residual compressive strain in the on-axis GaN film. This result supports the data from our PL and XRD studies presented earlier.

Additional evidence for the existence of residual compressive strain in the GaN films is the TEM contrast exhibited by the GaN films at distances of 50 - 80 Å from the interface with AlN. As can be seen in Fig. 9, the contrast reveals traces of rounded peaks and grooves, which are typical for films that are under compression [42,43]. Such near surface undulations are formed during heteroepitaxial growth by migration of the atoms deposited on the surface under the strain induced chemical potential gradients. From the same figure, it can be seen that at the groves the interplanar distances are smaller than at areas close to the peaks. This shows that there is a complementary compression at the areas close to the peaks.

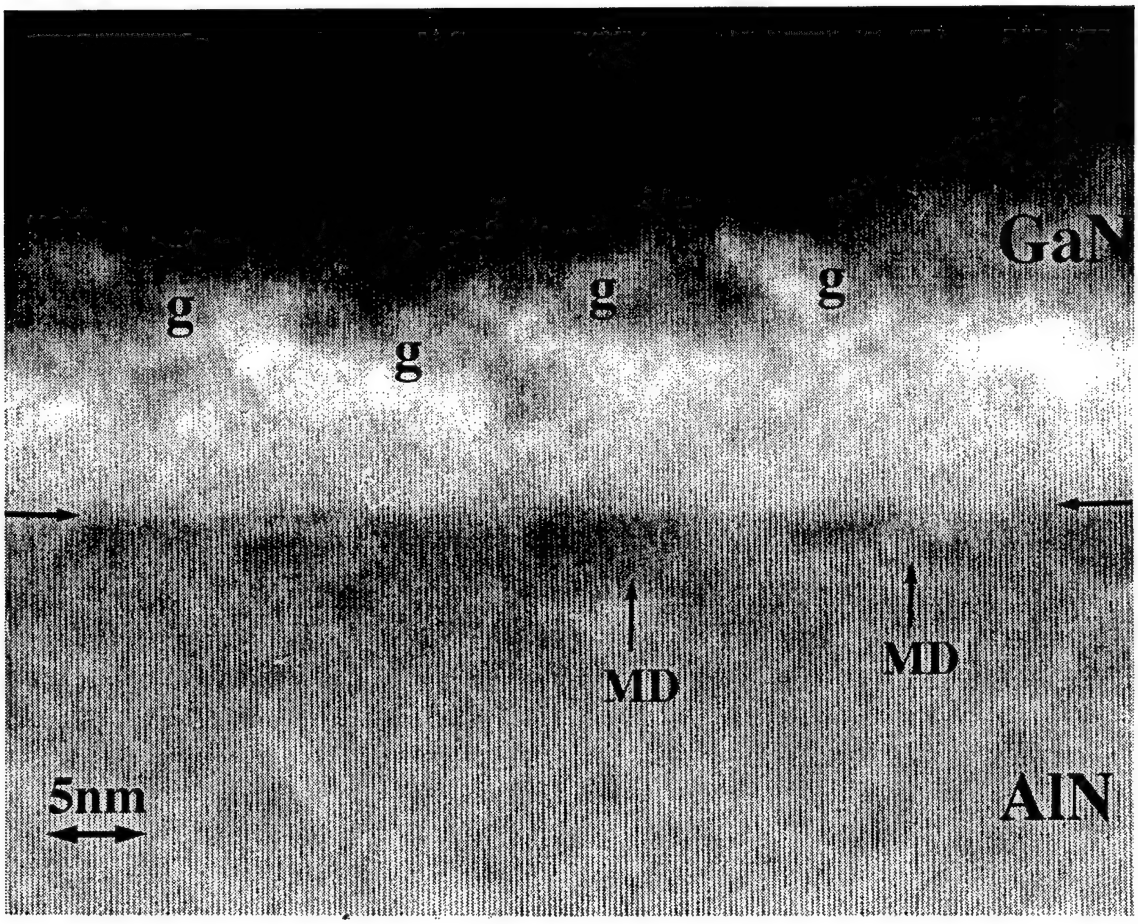

Figure 9. HRTEM micrograph from GaN/AlN interface of GaN/AlN 6H-SiC on-axis heterostructure. Note the extra-half planes in GaN films which are the misfit dislocations (MD) generated to relieve the misfit strain at that interface. The peaks and grooved are denoted by P and D.

Thus our HRTEM studies reveal the stress due to lattice mismatch is not fully relieved at the GaN/AlN for films grown on on-axis SiC. This results in a residual compressive stress that counteracts the tensile stress due to thermal mismatch. If this compressive stress is stronger then the GaN films should be in compression. This explains why the thin ($t \leq 0.6$ μm) GaN films grown on-axis films are in compression, while those grown concurrently on vicinal SiC wafers are in tension, with a maximum $\Delta c = 0.0072$ Å. As thickness increase ($t \geq 1$ μm) this compressive stress lessens, and at greater thicknesses ($t \geq 4$ μm) cracking may occur in the GaN to relieve thermal mismatch stress.

D. Conclusions

Compressive strain in GaN films grown on AlN/6H-SiC(0001) is reported for the first time. Residual biaxial strains determined in the films was due both to mismatches in thermal expansion coefficients and lattice parameters. A linear dependence due to this strain was

determined between E_{BX} and c for 22 GaN films grown on AlN/6H-SiC, and expressed by $E_{BX} = (-14.912 + 3.545*c)$ eV. Poisson's ratio for GaN was determined to be $\nu = 0.18$ from values of c and a for 22 GaN films. The shift of E_{BX} with biaxial film stress was estimated to be 23 meV/GPa. A marked variation in E_{BX} and c was observed for GaN films grown concurrently on AlN buffers and vicinal and on-axis SiC wafers. This variation was greatest for films ≤ 0.6 μm thick, where a maximum shift of $\Delta E_{BX} = 17$ meV and $\Delta c = 0.0072$ Å was observed, and the samples on the on-axis SiC were in compression.

Related TEM results showed a higher density of steps on the vicinal SiC wafers. These steps acted as formation sites for inversion domain boundaries (IDBs). Threading dislocation densities of ~10^{10}/cm^2 and ~10^8/cm^2 were observed for GaN on AlN grown vicinal and on-axis SiC, respectively. The on-axis SiC substrate did not contain sufficient steps for defect formation to fully relieve the lattice mismatch via defect formation at the GaN/AlN and AlN/SiC interfaces at the growth temperature. This resulted in residual compressive stresses that counteracts the tensile stresses that formed upon cooling due to the mismatch in thermal expansion coefficients. A 0.9% residual compressive strain at the GaN/AlN interface was calculated by comparing the average experimental lattice mismatch at the interface (1.6%) observed via HRTEM with that theoretically predicted for GaN/AlN (2.5%). It is proposed that this strain was accommodated elastically and resulted in biaxially compressive stresses in the films.

E. Future Research Plans and Goals

Raman Spectroscopy will be used to confirm that some of the GaN films in this study have compressive residual strain. The initial results are promising, and in the next report they will be presented in full detail. GaN films grown by other systems in our group, most notably MBE grown material, will tested by PL and XRD to see if they fit the model presented for E_{BX}, as well as the calculation of Poisson's ratio. In addition, two additional GaN films on sapphire will be tested.

F. References

1. H. Amano, K. Hiramatsu, and I. Akasaki, Jpn. J. Appl. Phys. **27**, L1484 (1988)
2. Detchprohm, K. Hiramatsu, K. Itoh, and I. Akasaki, Jpn. J. Appl. Phys. **31**, (10B) L1454 (1992).
3. K. Hiramatsu, T. Detchprohm, and I. Akasaki, Jpn. J. Appl. Phys. **32**, 1528 (1993).
4. I. A. Buyanova, J. P. Bergman, B. Monemar, H. Amano, and I. Akasaki, Appl. Phys. Lett. **69**, 1255 (1996).
5. X. J. Ning, F. R. Cein, P Pirouz, J. W. Yang, and M. A. Khan, J. Mater. Res. **11**, 580 (1996).
6. T. W. Weeks, M. D. Bremser, K. S. Ailey, E. Carlson, W. G. Perry, and R. F. Davis, Appl. Phys. Lett. **67**, 401 (1995).
7. T. W. Weeks, M. D. Bremser, K. S. Ailey, E. Carlson, W. G. Perry, E. L. Piner, N. A. El-Masry, and R. F. Davis, J. Mater. Res. **11**, 1011 (1996).

8. S. Tanaka, PhD dissertation, North Carolina State University, 1993.
9. W. Li and W. Ni, Appl. Phys. Lett. **68**, 2705 (1996).
10. S. Krishnankutty, R. M. Kolbas, M. A. Khan, J. N. Kunzia, J. M. Van Hove and D. T. Olson, J. of Electron. Mat. **21**, 609 (1992).
11. J. W. Orton, Semicond. Sci. Technol. **11**, 1026 (1996).
12. B. Monemar, J. P. Bergman, I. A. Buyanova, H. Amano, I. Akasaki, K. Hiramatsu, N. Sawaki, and T. Detchprohm, presented at the Topical Workshop on III-V Nitrides, Nagoya, Japan (1995).
13. C. Merz, M. Kunzer, U Kaufmann, I Akasaki and H. Amano, submitted to Phys. Rev. B., 1995
14. P. Boguslawski, E. Briggs, T. A. White, M. G. Wensell, and J. Bernholc, Mat. Res. Soc. Symp. Proc. **339**, 693 (1994).
15. J. Neugebauer and C. G. Van de Walle, Phys. Rev. B **50**, 8067 (1994).
16. P. Boguslawski, E. Briggs, J. Bernholc, Phys. Rev. B **51**, 17255 (1995).
17. W. Shan, R. J. Hauenstein, A. J. Fisher, J. J. Song, W. G. Perry, M. D. Bremser, R. F. Davis and B. G. Goldenberg, submitted to Phys. Rev. B
18. D. Volm, K. Oetinger, T. Streibl, D. Kovalev, M. Ben-Chorin, J. Diener, B. K. Meyer, J. Majewski, L. Eckey, A. Hoffman, H. Amano, I Akasaki, K. Hiramatsu, and T. Detchprohm, Phys. Rev. B **53**, 16543 (1995).
19. L. Eckey, J. C. Holst, P. Maxim, R. Heitz, A. Hoffmann, I. Broser, B. K. Meyer, C. Wetzel, E. N. Mokhoc, and P. G. Baranov, Appl. Phys. Lett. **68**, 415 (1996).
20. P. F. Fewster and N. L. Andrew, J. Appl. Cryst. **28**, 451 (1995).
21. J. C. Braveman and R. Sinclair, J. Electron Microsc. Technique 1, 53, (1984).
22. G. M. Ma and S. Chevaharoencul, MCNC Technical report TR90-33 (1990).
23. W. Shan, B. D. Little, A. J. Fischer, J. J. Song, B. Goldenberg, W. G. Perry, M. D. Bremser and R. F. Davis, to be submitted.
24. C. M. Balkas, C. Basceri, and R. F. Davis, Powder Diffraction **10**, 266 (1995).
25. E. Burnstein, Phys. Rev. **93**, 632 (1954).
26. A. Gassmann, T. Suski, N. Newman, C. Kisielowski, E. Jones, E. R. Weber, A. Liliental-Weber, M. D. Rubin, H. I. Heleva, I. Grzegory, M. Bockowski, J. Jun, S. Porowski, J. Appl. Phys. **80**, 2195 (1996).
27. B. Monemar, Phys. Rev. B **10**, 676 (1974).
28. K. Pakula, A. Wysmolek, K. P. Korona, J. M. Baranowski, R. Stepniewski, I. Grzegory, M. Bockowski, J. Jun, S. Krukowski, M. Wroblewski, and S. Porowski, Solid State Commun. **97**, 919 (1996).
29. K. N. Tu, J. W. Mayer, and L. C. Feldman, in *Electronic Thin Film Science*, (Macmillan, New York 1992) p. 84.
30. V. A. Savastenko and A. U. Sheleg, Phys. Status Solidi A **48** 135 (1978)
31. T. Azuhata, T. Sota, K. Suzuki, J. Phys.: Condens. Matter **8**, 3111 (1996)
32. C. Kisielowski, J. Krüger, S. Rumimov, T. Suski, J. W. Ager III, E. Jones, Z. Liliental-Weber, M. Rubin, E. R. Weber, M. D. Bremser and R. F. Davis, to be submitted to Phys. Rev. B, 1996.
33. *Landolt-Börnstein*, edited by O. Madelung (Springer, New York, 1982), Vol. 17.
34. K. Kim, W. R. L. Lambrecht, and B. Segall, Phys. Rev. B **50**, 150 (1994).
35. A. Polian, M Grimsdich, and I. Grzegory, J. Appl. Phys. **79**, 3343 (1996).
36. W. Shan, T. J. Schmidt, R. J. Hauenstien, J. J. Song and B. Goldenberg, Appl. Phys. Lett. **66**, 3492 (1995).
37. P. Perlin, I. Gorczyca, N. E. Christensen, I. Grzegory, H. Teisseyre, and T. Suski, Phys. Rev. B 45, 13 307 (1992).
38. W. Rieger, T. Metzger, H. Angerer, R. Dimitrov, O. Ambacher, M. Stutzmann, Appl. Phys. Lett. **68**, 970 (1995).
39. Pirouz P, et. al. Nitride Workshop on Wide Bandgap Nitrides, St. Louis, (1996)
40. A. Westwood, R. Youngman, M. McCartney, A. Cormack and M. Notic, J. Mater. Res. **10**, 1270 (1995).

41. F. Chien, X. Jing, P. Pirouz, M. D. Bremser, and R. F. Davis, Appl. Phys. Lett. **68**, 2678 (1996).
42. C. Roland, MRS Bulletin **21**, 27 (1996).
43. A. Cullis, MRS Bulletin **21**, 21 (1996).

VI. Dry Etching of Gallium Nitride

A. Introduction

Gallium nitride is a wide bandgap semiconductor which has applications such as short wavelength light emitters and detectors, high temperature, frequency, and power electronics [1,2]. A crucial step in creating these devices is to etch anisotropic features in the GaN. Wet etching has been employed in many semiconductor processes. Thus far, wet etching has produced poor results on GaN, such as slow etch rate and isotropic etch profiles [3]. Both of these characteristics are undesirable for commercial applications. As technology advances, the need for anisotropic etch profiles increases to accommodate a smaller, more densely packed network of devices. Dry etching is an attractive alternative to wet etching. Varying degrees of anisotropy along with high etch rates can be achieved using different dry etch techniques.

There are four primary dry etch techniques that have been employed on GaN. They are Reactive Ion Etching (RIE), Electron Cyclotron Resonance Etching (ECR), Magnetron Enhanced Reactive Ion Etching (MIE), and Inductively Coupled Plasma Etching (ICP). Out of the four techniques, RIE produces the slowest etch rates and lowest degree of anisotropy [4-6]. ECR, which has had much attention from Pearton *et al.* [1,3,7-8], produces significantly better results than RIE. MIE, was employed by McLane *et al.* [2], and produced results comparable to that of ECR etching. Inductively coupled plasma etching is the newest addition to the dry etching techniques of GaN. Shul [9] has shown that ICP can produce etch characteristics similar to that of ECR.

The objectives of this report are to discuss recent advances in etching GaN with the three techniques of dry etching. In the following sections, each of the etching techniques will be discussed and compared, along with a discussion of the work being done etching GaN in our labs and the results to date.

B. Etching Overview

As previously stated, each of the three primary dry etch techniques will be discussed. They will be presented individually, and then compared at the end of this section.

Reactive Ion Etching. As the III-V nitride technology advances, the need for commercially viable processes is getting more important. In this case, a commercially viable etching process would be one that produces the fastest controllable etch rate along with etch profiles that are suitable for the desired electronic device. Reactive ion etching is lacking in both of these areas. The reason for these shortcomings are the parameters that are involved in the process. Reactive ion etching is generally performed at pressures between 10 and 100 mTorr [4-6]; at these pressures, the mean free path of the bombarding ions is between 5 and .5 mm, respectively. With mean free paths this small, the bombarding ions will hit other ions and scatter. This

scattering will result in the ions not hitting the GaN surface at 90° angles, resulting in a lesser degree of anisotropy than is usually desired. There are some cases where isotropic etch profiles are desired, but for the most part, anisotropic etch profiles are desired.

Etch rate is another area where RIE has fallen behind the other two methods. Lin *et al.* [4] have reported the highest etch rate to date via RIE of 105 nm/min in a BCl_3 plasma. This is actually a fairly high etch rate, but at what cost? The parameters were 15 sccm BCl_3, 10 mTorr pressure, 150 w RF power, and -600 v dc bias. The etch rate is in part a function of the dc self bias and the energy of the bombarding ions is also a function of the dc self bias. As the ion energy increases, there is a better the chance of etch induced damage to the surface of the material. There have been no etch induced surface damage studies on GaN reported to date. Murtagh *et al.* [10] showed via photoreflectance spectroscopy that the larger the dc self bias, the greater the surface damage to GaAs. Even though GaN is a much stronger material than GaAs, it could still undergo the same damage as GaAs, just to a lesser extent.

Electron Cyclotron Resonance Etching. Out of the major types of etching GaN, ECR has the most widespread use in the research field. Shul *et al.* [9] have recently obtained etch rates of 900 nm/min in a Cl_2/H_2/ Ar plasma using ECR etching. One of the reasons for the high etch rates is that ECR produces a high density plasma, which results in higher etch rates as compared to RIE. The plasma in an RIE is everywhere in the chamber between the source and ground. In an ECR etching system, the plasma is magnetically confined by permanent magnets on the outside of the chamber.

The potential for surface damage to the material is reduced in an ECR etcher. ECR etching uses a microwave source instead of a RF source to produce the plasma, and a separate RF source on the substrate to bias the substrate. Since the microwave source produces a high density plasma, a lower bias is required to etch the material. With a lower dc bias on the substrate, the energies of the ions bombarding the surface of the material is in turn lowered. This reduces the risk of producing etch induced surface damage.

Magnetically Enhanced Reactive Ion Etching. The major difference between RIE and MIE is that the plasma is magnetically confined in an MIE etcher. The magnetic field confines the plasma around the cathode that the sample is on. This in turn increases the etch rate and lowers the dc bias. Along with other things, the dc bias is a function of the surface area of the ground. Since the plasma is confined, the surface area of the ground that the plasma is exposed to is significantly reduced. McLane *et al.* [2] have reported etch rates of 350 nm/min using a BCl_3 plasma which is the highest reported to date.

Inductively Coupled Plasma Etching. A newcomer to etching GaN, ICP has already proven to have much potential as the best etching technique for GaN. Etch rates over 7000Å/min have been achieved by Shul [9] using Cl_2/H_2/Ar chemistries in a commercial ICP system. Like ECR, ICP produces a high density plasma and has a separate RF source on the substrate to

control the dc bias. ICP has some distinct advantages over ECR etching, such as better control of plasma density, higher operating pressures, more economical, and more easily scaled up to production.

The above has been a brief description of the four primary dry etch techniques for GaN. The ICP, ECR, and MIE improve upon three major faults of RIE; namely the slow etch rate, surface damage, and isotropic etch profiles. Table I is a summary of the four different etching methods and some typical etching parameters along with the corresponding etch rates.

Table I. Etch Rate Parameters for Dry Etching of GaN

Maximum Etch Rate (nm/min)	Plasma Gasses	Pressure (mTorr)	Power (watts)	DC Bias (- volts)	Reference
700	$Cl_2/H_2/Ar$	1	750	280	[9] ICP
900	NM#	1	1000	290	[9] ECR
285	$Cl_2/H_2/CH_4/Ar$	2	275	NM#	[11] ECR
110	Cl_2/H_2	1	1000	150	[1] ECR
110	$HI/H_2/Ar$	1	1000	150	[8] ECR
90	$HBr/H_2/Ar$	1	1000	150	[8] ECR
350	BCl_3	7	NM#	100	[2] MIE
105	BCl_3	10	150	231	[4] RIE
60	HBr/Ar	50	NM#	350	[6] RIE
50	$SiCl_4/Ar$	20	NM#	400	[5] RIE

NM# designates a parameter that was not mentioned in the reference.

C. Experimental Procedure

Experimental Apparatus. Figure 1 shows the basic etching setup. It consists of an inductively coupled plasma etcher, gas handling/storage, gas scrubber, optical emission spectrometer, and Laser Reflectance Interferometer. The etcher consists of a custom designed and built stainless steel chamber with a loadlock, with a water cooled anodized aluminum cathode. A 2000w 13.56 MHz power generator and autotuning matching network provide power to the inductive source antennae for plasma generation. Pressure in the chamber is monitored by an MKS 627A Capacitance Manometer. A Leybold mechanical pump and an Alcatel turbomolecular pump maintain the proper level of vacuum required for processing along with a base pressure of 4E-7 Torr.

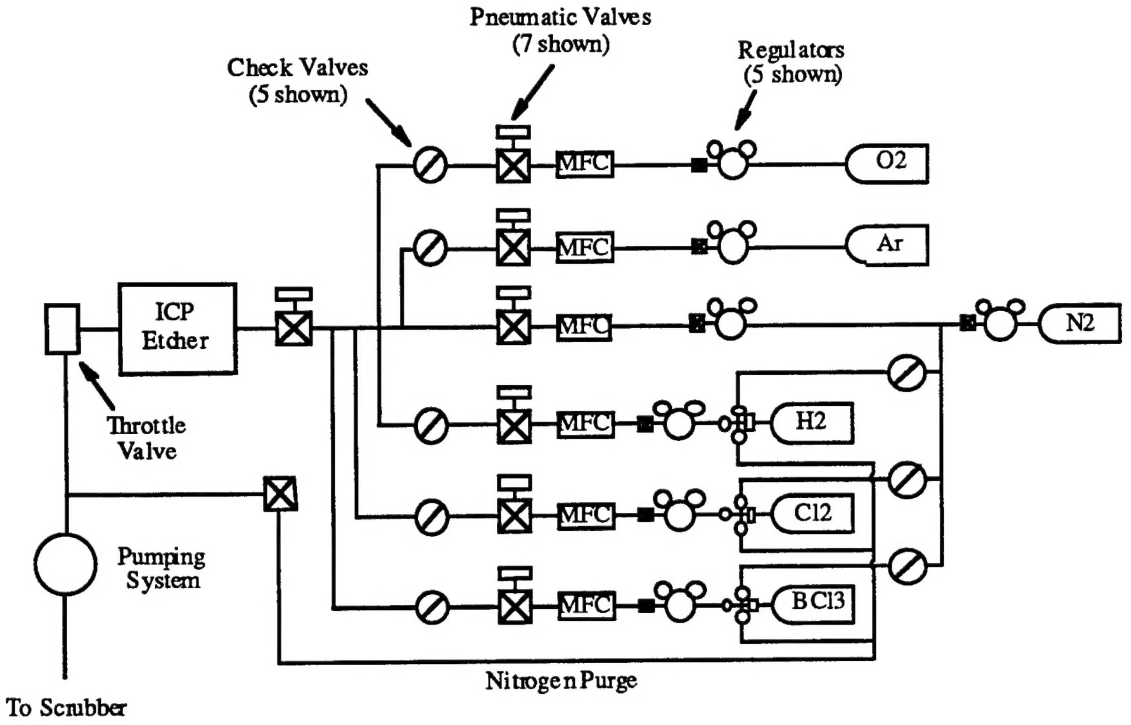

Figure 1. ICP schematic diagram.

Choice of Process Gasses. The gasses that the etching system will be capable of using are BCl_3, Cl_2, H_2, O_2, N_2, and Ar. Chlorides have proven to be effective gasses to etch GaN [1,2,4,8,11].

Etching Procedure. An etching procedure has not yet been fully developed. Photoresist is still being tested as an etch mask. It was originally thought to work well, but further testing has shown erosion of the photoresist.

The analytical tools that are used to characterize the etch are a profilometer for the step height, an SEM for the slope of the step, AFM for the surface roughness, and AES/XPS to observe the residual gas species on the sample surface. Schottky contacts are also going to be deposited to see how etching affects the barrier height, ideality factor, and leakage current [12].

D. Results and Discussion

Construction is complete for the new ICP etching system. Minor finishing details are being tended to and tests are being performed.

Preliminary results have shown etch rates of 4400Å/min. using $Cl_2/Ar/H_2$ for the process gasses. The surfaces look smooth under an SEM with sidewall of approximately 55° with 90° being vertical. Figure 2 shows a typical etch profile obtained in the preliminary studies. The reason for the slope of the etch appears to be erosion of the photoresist mask. If the sidewalls of the photoresist mask are not vertical, then the resultant profile of the etch will not be vertical.

Figure 3 shows an example of this effect. The original mask was 1μm thick and eroded down to approximately .3μ thick. Figure 4 shows an etched sample from the edge of the sample where the photoresist is thicker. The sidewall is closer to being vertical than in Figs. 2 and 3.

E. Future Research

Once the problem of mask erosion is worked out, parametric studies will be done varying the process gas and flow rates, ICP and RF power, and pressure to determine which combination yields the fastest etch rates and least surface damage/contamination. This will be aided as with the use of Laser Reflectance Interferometry to get *in situ* etch rates. Optical emission spectroscopy will be used to aid in the understanding of the plasma chemistry when

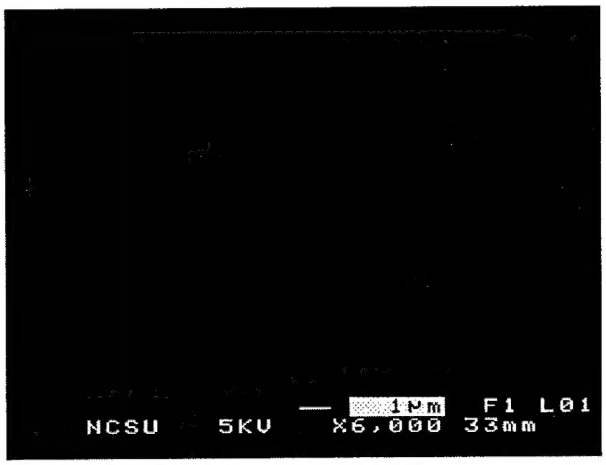

Figure 2. Typical etch profile obtained in the preliminary studies.

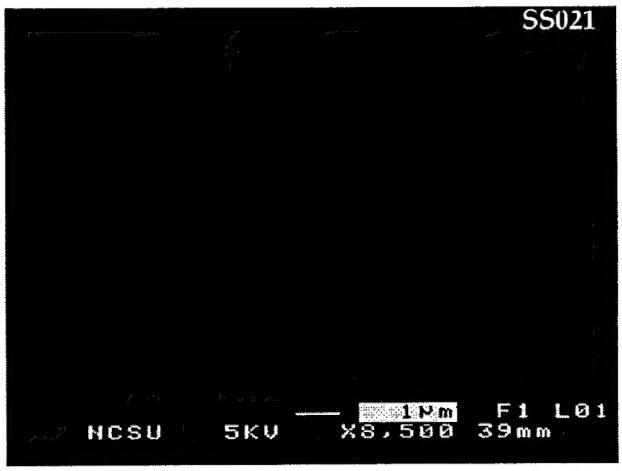

Figure 3. The resultant profile of the etch will not be vertical if the sidewalls of the photoresist mask are not vertical.

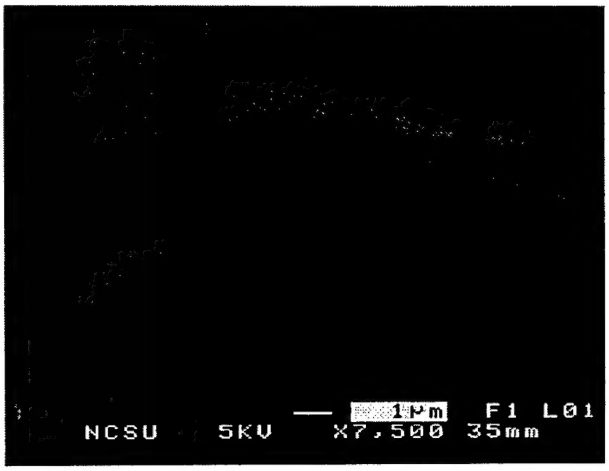

Figure 4. Etched sample from the edge of the sample where the photoresist is thicker.

etching the III-N materials. The primary gasses are going to be chlorides, but the use of other gasses may be explored. Surface analysis techniques will be employed to determine the roughness of the surface, etch profiles, step height, and surface contamination. Since the end product of the III-N research is electronic devices and optoelectronic devices, knowing the effects of etch induced surface damage is very important. If an etched surface is highly contaminated or very rough, it may not be good for electronic and optoelectronic devices. Determining the surface effects is equally important as determining the etch rates. Other effects such as heating or cooling the sample may also be explored. The ultimate goal of this research is to etch anisotropic features with etch rates suitable for industry, and damage/contamination free etch surfaces.

F. References

1. S. J. Pearton, C. R. Abernathy, F. Ren, Appl. Phys. Lett. **64**, 2294 (1994).
2. G. F. McLane, L.Casas, S. J. Pearton, C. R. Abernathy, Appl. Phys. Lett. **66**, 3328 (1995).
3. S. J. Pearton, C. R. Abernathy, F. Ren, J. R. Lothian, P. W. Wisk, A. Katz, J. Vac. Sci. Technol. A **11**, 1772 (1993).
4. M. E. Lin, Z. F. Fan, Z. Ma, L. H. Allen, H. Morkoc, Appl. Phys. Lett. **64**, 887 (1994).
5. I. Adesida, A. Mahajan, E. Andideh, Appl. Phys. Lett. **63**, 2777 (1993).
6. A. T. Ping, I. Adesida, M. A. Khan, J. N. Kuznia, Electronics Letters **30**, 1895 (1994).
7. S. J. Pearton, C. R. Abernathy, F. Ren, J. R. Lothian, P. W. Wisk, A. Katz, C. Constantine, Semicond. Sci. Technol. **8**, 310 (1993).
8. S. J. Pearton, C. R. Abernathy, C. B. Vartuli, Electronics Letters **30**, 1985 (1994).
9. R. J. Shul, Presentation Viewgraphs
10. M. Mortagh, P. V. Kelly, P. Herbert, M. O'Connor, G. Duffy, G.M. Crean, Applied Surface Science **63**, 158 (1993).
11. R. J. Shul, A. J. Howard, S.J. Pearton, C.R. Abernathy, C.B Vortuli, P.A. Barnes, M. J. Bozack, J. Vac. Sci. Technol. B **13**, 2016 (1995).
12. G. F. McLane, W. R. Buchwald, Mat. Res. Soc. Symp. Proc. **340**, 221 (1994).

VII. Distribution List

Dr. Colin Wood Office of Naval Research Electronics Division, Code: 312 Ballston Tower One 800 N. Quincy Street Arlington, VA 22217-5660	3
Administrative Contracting Officer Office of Naval Research Regional Office Atlanta 101 Marietta Tower, Suite 2805 101 Marietta Street Atlanta, GA 30323-0008	1
Director, Naval Research Laboratory ATTN: Code 2627 Washington, DC 20375	1
Defense Technical Information Center Bldg. 5, Cameron Station Alexandria, VA 22304-6145	2